A Finite Element Model of Grain Boundary Sliding for Nanostructured Metals

by

Antoine Jérusalem

Submitted to the Department of Aeronautics and Astronautics
in partial fulfillment of the requirements for the degree of

Master of Science in Aeronautics and Astronautics

at the

MASSACHUSETTS INSTITUTE OF TECHNOLOGY

May 2004 [June 2004]

Author .....
Department of Aeronautics and Astronautics
May 14, 2004

Certified by .....
Raúl Radovitzky
Assistant Professor
Thesis Supervisor

Accepted by ....
Edward M. Greitzer
H.N. Slater Professor of Aeronautics and Astronautics
Chair, Committee on Graduate Students

A Finite Element Model of Grain Boundary Sliding for Nanostructured Metals

by

Antoine Jérusalem

Submitted to the Department of Aeronautics and Astronautics
on May 14, 2004, in partial fulfillment of the
requirements for the degree of
Master of Science in Aeronautics and Astronautics

Abstract

Nanocrystalline metals, i.e., polycrystalline metals with grain sizes in the nanometer range, have elicited significant interest recently due to their potential for achieving higher material strength in combination with increased formability at lower temperatures and higher strain rates, among other potential performance improvements in the material properties. In addition, there is a growing body evidence of unique deformation mechanisms furnishing a qualitatively different mechanical behavior in materials structured at the nanometer scale. In particular, the expected increase of the yield strength with the refinement of the microstructure appears to level off at grain sizes of the order of 10 to 50 nm and reverts to a decrease of strength with further reduction of grain size. Experimental studies and atomistic simulations have provided evidence of this peculiar behavior.

In this work, we propose a continuum model describing the competing deformation mechanisms believed to determine the effective response of nanocrystalline materials. A phenomenological model considering grain boundary sliding and accommodation as uncoupled plastic dissipative deformation mechanisms is formulated to describe the constitutive behavior of grain boundaries. Tensile test simulations using the proposed model reproduce the inverse trend in the grain-size dependency of the macroscopic yield stress predicted by atomistic simulations and experiments. Even more noteworthy is the finding that the numerically predicted grain-size dependency of the yield stress shows a linear relation to the inverse square root of the grain size, a phenomenon identified as the inverse Hall-Petch effect. The importance of this result is lastly enhanced by the prediction from the model that the observed discrepancy between molecular dynamics and experimental results may be strongly related to the deformation rate.

Thesis Supervisor: Raúl Radovitzky
Title: Assistant Professor

Acknowledgments

I would like to thank my advisor, Prof. Radovitzky, for his guidance through this project, taking me away from Toulouse, la ville rose, and bringing me to Boston, la ville blanche.

The support of the NNSA ASC Academic Alliance Program under contract no. W-7405-ENG-48, subcontract no. B523297 is gratefully acknowledged.

I am eternally grateful to all of TELAC students who courageously let me scream in the office while following soccer on the internet. I am especially thankful for Kevin and Jeremy who bravely went through my thesis as crash-testers.

I of course thank my parents, my four sisters Céline, Christelle, Laure and Claire, my grand-parents (Manou, I am sure that from where you are, you are still following all of my steps) and all my family who have helped me in the difficult periods and sustained me in the good ones, always close to me despite the Atlantic Ocean.

I do not forget my friends back in France that I cowardly left for the country of Mickey Mouse and hamburgers, and those who are now working all over the world.

I would finally like to thank all of my friends in Boston (including the ones who just left) for all the fun that they brought and keep bringing to my life and, of course, Farinaz for her help and patience during this long year of PhD qualifiers, stress and thesis.

Contents

List of Figures

List of Tables

Chapter 1

Introduction

Nanocrystalline metals are materials with a polycrystalline structure and grain sizes in the nanometer range. Nanocrystalline materials have elicited significant interest recently due to their potential for achieving higher material strength in combination with increased formability at lower temperatures and higher strain rates, among other potential performance improvements in the material properties [1, 2, 3, 4, 5, 6]. Efforts to characterize and understand the mechanical behavior of these materials have unveiled some unique features of deformation that are not commonly observed in polycrystals. It appears that the growing importance of grain-boundary deformation mechanisms in materials structured at the nanometer scale is responsible for this departure from the mechanical behavior of conventional polycrystalline materials. It is therefore important and opportune to devise theories describing the peculiar mechanical behavior of nanocrystals.

Conventional polycrystals have long been known to exhibit a strong dependence of the yield stress on the grain size. This behavior has been observed to agree with the Hall-Petch [7, 8] relation:

$$\sigma_y = \sigma_0 + kd^{-\frac{1}{2}} \tag{1.1}$$

where k is a positive multiplicative constant and σ_0 is the lattice friction stress.

Based on this observation, microstructure refinement has been exploited as a means of producing materials with increased strength. There has since been specu-

lation as to the limits of the Hall-Petch relation. The first observations of deviations from the Hall-Petch law were given in the pioneering work of Chokshi *et al.*[9]. They observed a decrease of the yield stress when the grain size was reduced from $16nm$ to $7nm$ in copper and palladium, see Figure 1-1. More curiously, their observations of the dependence of the yield stress on grain size also appeared to follow an inverse square root relation, Equation 1.1, but with a negative coefficient k. There has since been significant efforts to confirm and explain this inverse—sometimes also referred to as reverse—Hall-Petch effect. A literature survey of experimental results on a variety of nanocrystalline metals is provided in Appendix A. The most accepted

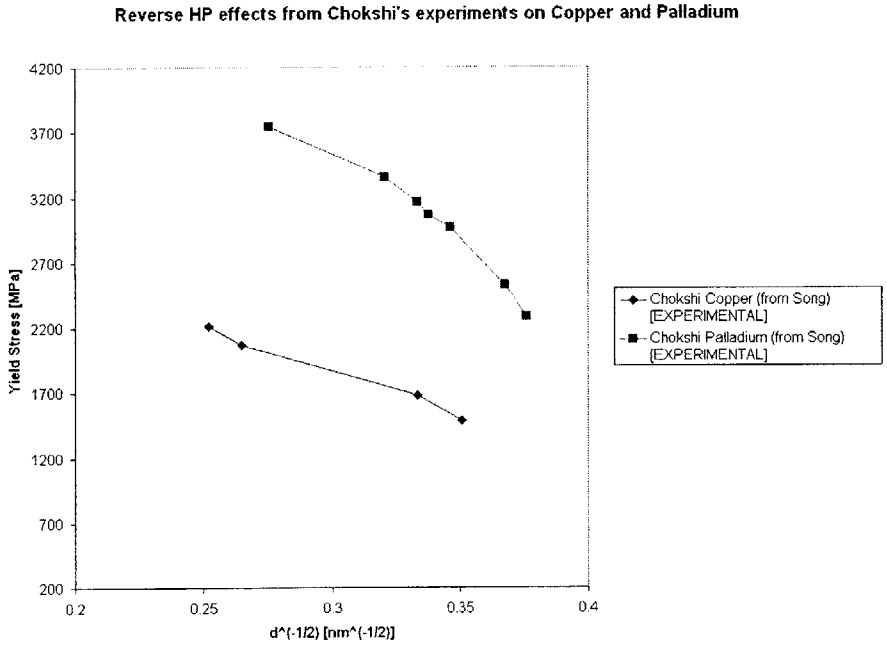

Figure 1-1: Chokshi's experimental observation (1989) [9] of the reverse Hall-Petch effect on Copper and Palladium (yield stress data taken from Song's paper [10])

explanation of the direct Hall-Petch (HP) effect is a hardening mechanism characterized by the pile-up of lattice dislocations at the grain boundaries. As the grain size decreases, there is smaller room for dislocation activity inside the grains, whereas the relative volume fraction of grain boundary atoms increases. This suggests a qualitative change in the operative deformation mechanisms from dislocation-mediated plasticity to grain-boundary deformation mechanisms. Different grain boundary de-

formation mechanisms explaining this change of behavior have been proposed. Chokshi *et al.* suggested that Coble creep at room temperature is perhaps the mechanism explaining their experimental results [9]. But more recent molecular dynamics simulations on copper by Schiøtz *et al.* have shown a reverse Hall-Petch Effect in the absence of thermally activated processes [11], see Figure 1-2. Atomistic simulations [12, 11, 13, 14, 15] have shown that the main deformation mechanism taking place at grain boundaries consists of localized sliding accompanied by some accommodation mechanism that maintains the intergrain compatibility at triple points, for example. However, there is still dissent on the nature of this accommodation process. Recent

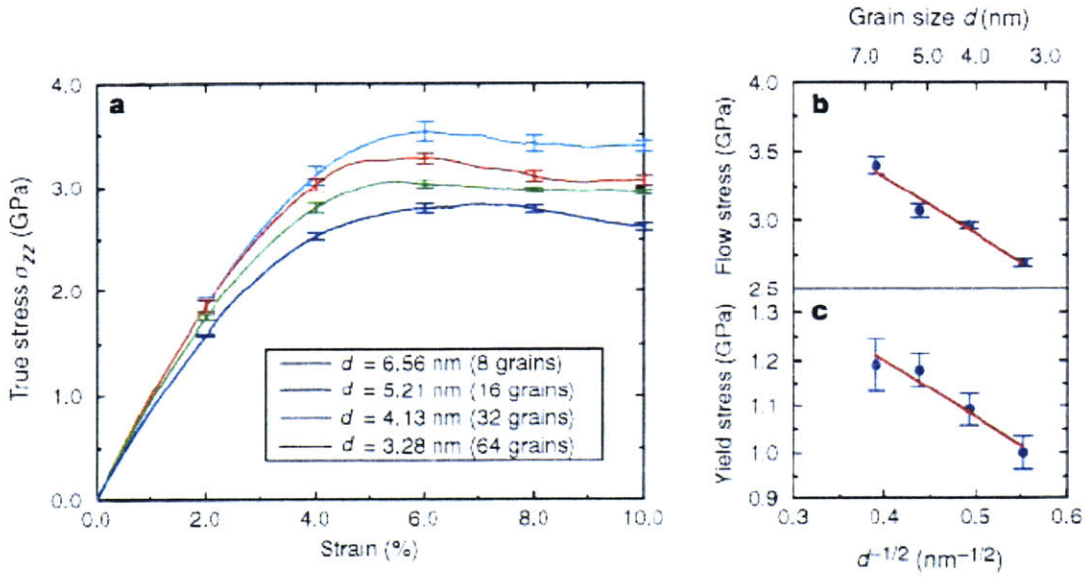

Figure 1-2: Schiøtz' molecular dynamics simulations (1998) showing the reverse Hall-Petch Effect [11]

large-scale atomistic simulations have been able to show the crossover from the direct to the inverse grain-size dependency in the material strength [16], see Figure 1-3). Experimental studies have also provided evidence of this peculiar behavior, see for example [17, 2, 18, 1] and many other references in Appendix A. However, due to the difficulty of interpreting the experimental results and the impossibility of eliminating material impurities and controlling the material densities with current processing methods, the results are often not reproducible and, therefore, not conclusive.

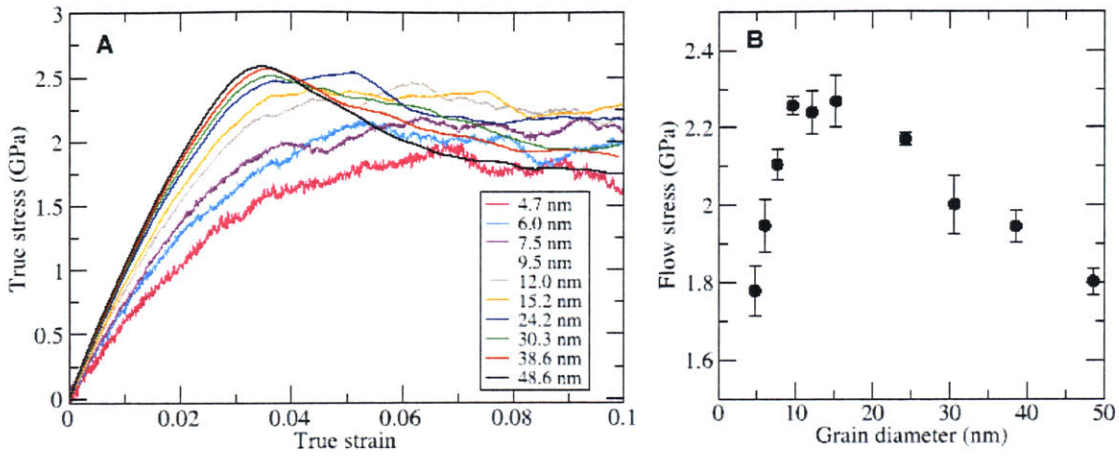

Figure 1-3: Schiøtz' molecular dynamics simulations (2003) showing the crossover from the direct to the reverse Hall-Petch Effect [16]

Summarizing the experimental and theoretical findings, there is a growing consensus that the apparent anomalous dependence of yield stress on grain size can be rationalized by the activation of deformation mechanisms taking place at the grain boundary which compete with crystal plasticity and become the dominant operative dissipative deformation mechanism when grain sizes are sufficiently small.

In this work, we propose a continuum model describing the competing deformation mechanisms that are believed to determine the effective response of nanocrystalline materials. The model consists of a finite element formulation of the continuum three dimensional problem with a special treatment of the boundaries between grains. Following what has been observed experimentally, grain boundaries are considered as having a finite size. Interface elements inspired by well-established descriptions of fracture and crack propagation [19] are formulated to account for the special kinematics of grain boundaries (i.e., to describe grain boundary sliding and other accommodation mechanisms). A phenomenological model considering grain boundary sliding and accommodation as uncoupled plastic dissipative deformation mechanisms is formulated to describe the constitutive behavior of grain boundaries. The model essentially considers the grain boundary as a slip plane in a similar manner to crystal plasticity models but, without a preferred slip direction. The opening mode is

modeled with a similar plasticity formulation.

In Chapter 2, the proposed continuum model of the deformation of nanocrystalline materials is described in detail, including the continuum framework, the constitutive models and the numerical approach. Special emphasis is given to the constitutive model of grain boundary sliding and accommodation. In Chapter 3, first the model parameters are calibrated using the experimental results of Sanders et al [20, 21] and subsequently the resulting calibrated model is used to conduct numerical simulations of the tensile response of nanocrystalline copper under a range of grain sizes and strain rates. The ability to use rather large computational meshes enables the investigation of grain-size dependency of the nanocrystal effective response. To this end, simulations of tensile tests are conducted on cubic-shape, $100nm$ and $20nm$ sized nanocrystalline copper specimens of grain sizes ranging from $33.33nm$ to $3.33nm$. The numerical results are compared to both experimental [20, 21] and molecular dynamics results [11]. In particular, vastly different strain rate conditions similar to published experimental and atomistic results are simulated in an attempt to ascertain if the continuum model is able to shed light on the significantly different yield strengths predicted by those two approaches.

Chapter 2

Continuum modeling of the mechanical behavior of nanocrystals

To a large extent, the mechanical behavior of nanocrystals has been modeled using large scale atomistic simulation. Whereas this approach has been extremely successful in unveiling the basic deformation mechanisms taking place in nanocrystals, the need to represent and account for the dynamics of each individual atom poses severe restrictions on the extent of the nanocrystalline sample sizes that can be achieved in the foreseeable future. For instance, only recently has it been possible to simulate grain and sample sizes that capture the transition from the inverse to the direct Hall-Petch effect, [16]. In addition, the time scales available to molecular dynamics simulation are also severely constrained by the need to track the dynamics of individual atoms. A common approach to circumvent this limitation is to impose extremely large deformation rates in the simulations ($10^{10}/sec$ and higher are not uncommon), which allows to reach significant values of strain in very short–picoscale—times. However, these strain rate levels are not realistic and it is not entirely clear what the implications of such loading conditions on a real material are.

In this work we explore a modeling approach based on a continuum description of the deformation fields using the conventional framework of continuum mechanics

and its numerical discretization using a finite element strategy. Barring a few notable exceptions, see [22] for example, the continuum approach has not been explored in the modeling of the mechanical response of nanocrystals.

It is important to recognize that in a continuum description selected deformation mechanisms are explicitly accounted for using specialized kinematics of the deformation and phenomenological constitutive models. Although it is not inconceivable to incorporate in the constitutive models lower scale features through a multiscale modeling approach, in this work we restrict our attention to purely phenomenological models whose parameters have to necessarily be calibrated to experimental characterizations. In the case of grain boundary effects in nanocrystals these subscale features include grain boundary migration, grain boundary diffusion and phenomena related to the creation, reflection or transmission of dislocations at the grain boundary.

The FEM formulation of the grain boundary clearly needs to be differentiated from that of the grain, in terms of the constitutive laws and the representation in finite elements. Finally, for the grain boundary, consideration should be given to the fact that grain boundary sliding may be coupled to another feature in order to take into account the "accommodation process".

2.1 Preliminaries

In many FEM simulations, Voronoï diagrams have generally been chosen to build a random distribution of grains, either in 2-D (or cylindrical 2-D) or 3-D. Nevertheless, this approach does not account for any stability or the physical features of the grains configuration. On the contrary, as Stevens [23] noticed in his paper of 1971 concerning Kelvin's 1887 study, a tetrakaidecahedron, Wigner-Seitz cell corresponding to body centered cubic lattices (See Figure 2-1), would be a high stable configuration for a polyhedral grain. Furthermore, for such a shape of grain, when doing a tensile or compression test along the z-axis in Figure 2-1, Stevens calculated that grain boundary sliding is at maximum compared to diffusion (75% of sliding for 25% of diffusion). Idealized grain morphologies resulting from the three dimensional packing

of tetrakaidecahedra are then adopted for simplicity as building blocks of nanocrystalline samples. This results in nanostructures consisting of equiaxed grains. Each grain is discretized using 192 second-order tetrahedral finite elements in a manner that leaves the overall polycrystal mesh conforming at the grain boundaries. Subsequently, interface elements are added at the boundaries between grains, taking advantage of the conformity of the existing mesh.

From now on, a "nxnxn" λ *nm specimen* will mean that the specimen is a cube of λ nm side length with a basic structure of n by n by n full grains (n in each three directions). For example, Figure 2-1 represents a 6x6x1 specimen ("1" grain in the z-direction and "6" in x- and y-directions). Consequently, a nxnxn specimen has a basis of n^3 full grains. Note that the configuration is then completed by other grains or halves, quarters and eighths of grains in order to complete the structure in a perfect cube (full grains between 4 other grains, halves on the facets of the cube, quarters, on the edges, and eighths in the corners). The direct consequence is that, in a "nxnxn" specimen, the total number of grains or pieces of grain will be of $n^3 + (n+1)^3$; e.g. if $n = 1$, this will give a total of 9 different crystals, and if $n = 6$, of 559 crystals. Finally, for the grains, 10-node (4 corner nodes and 6 mid-nodes) tetrahedra (cf. Figure 2-2) elements are used.

The next step is now to determine which metal will be used. In the light of all the work, both experimental and theoretical, that has already been done in this metal (cf. Figure A-1), copper was chosen.

As has been seen in the introduction, it seems that grain boundary sliding needs an "accommodation process" to be able to occur without any restriction. For instance, at the triple points or quadruple points, pure sliding is geometrically impossible, and sliding would be able to occur only with the help of grain deformation. Schiøtz [11] stated in 1998 that diffusion had not played any role in his MD simulations. On the other hand, Wolf *et al.* [24] argued that diffusion was a necessary process for sliding to occur, either in the grain (Nabarro-Herring diffusion) or in the grain boundary (Coble diffusion).

Another way of accommodating grain boundary sliding, namely opening, has often

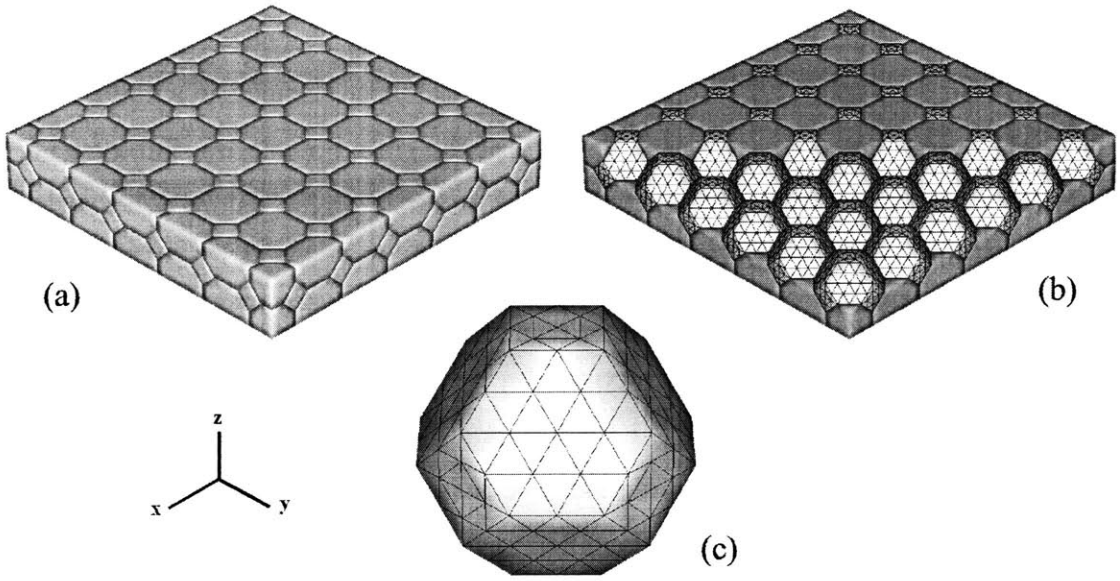

Figure 2-1: Tetrakaidecahedra in a 6x6x1 plate: the Subfigure (a) represents the complete plate where as the Subfigure (b) shows the same plate without some of the portions of grains on the top; finally Subfigure (c) gives a simple tetrakaidecahedron

been used in FEM. Fracture is known to occur after a threshold stress, and not as soon as a normal stress is applied to the grain boundary. Therefore, considering the opening as verifying a plastic law with a specific yield stress can be seen as a possibility. The same thing is also true for the sliding. As can be seen in Figure 2-4, the grain boundary is widening when subject to a tensile stress. Furthermore, its width, for a nanocrystal, is comparable to the size of the grains ($\sim$1 nm) [9]. Consequently, considering the grain boundary as a continuum material seems relevant and this approach was then chosen for the model.

Given that opening is coupled to sliding, the constitutive laws of both features need to be characterized. Among the first tests that have been done, a viscous law had been tried as suggested by Kê [25]. This law, however, did not take into account the plastic characteristics that have been observed in grain boundary sliding. This is why a 2D plastic law seems to be a better approach to define grain boundary sliding in the plane of the boundary. Another 1D plastic formulation was given to the opening, however, decoupled from the sliding's plastic law. The two laws were chosen to be

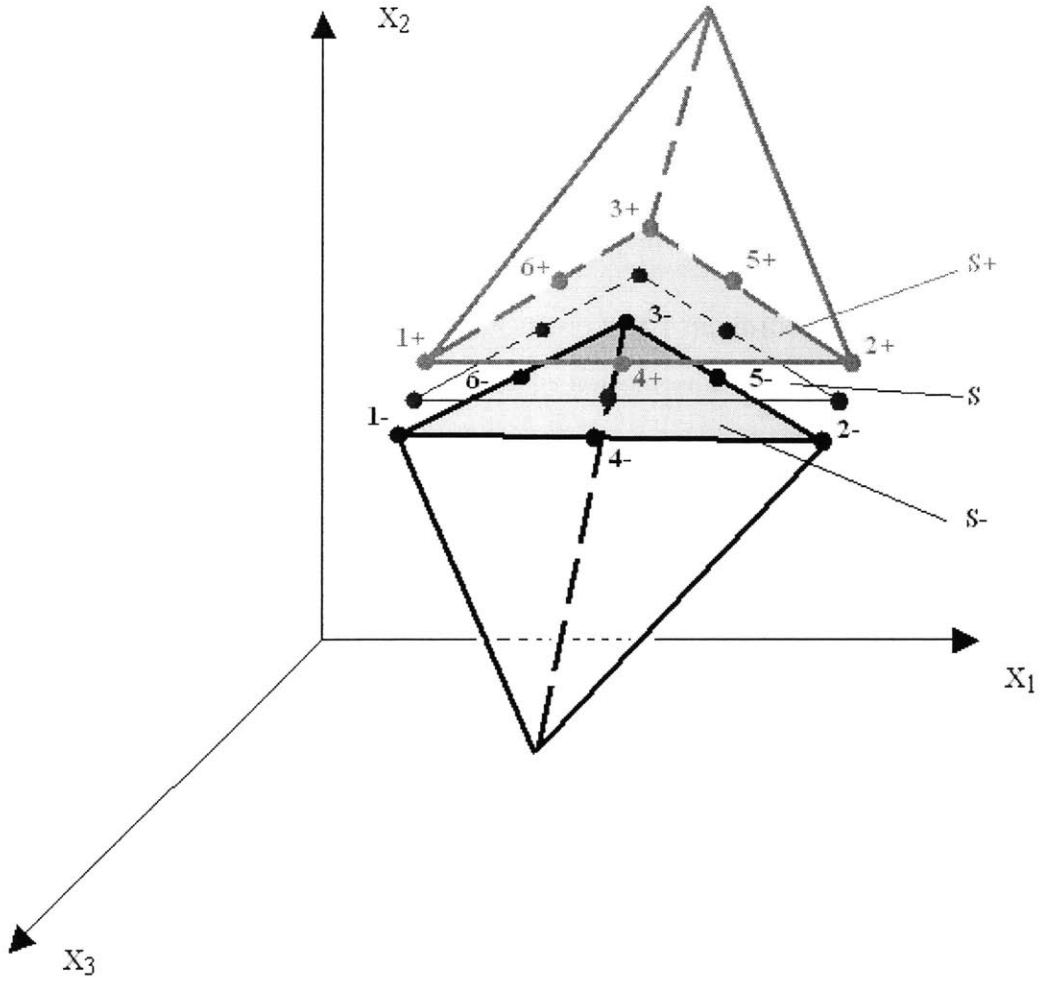

Figure 2-2: Two tetrahedra belonging to two different crystals separated by an interface element at the grain boundary: $S+$ and $S-$ correspond to the facets of the upper and lower tetrahedra and S, to the midsurface

the same; the only difference (except for the dimension) was that, for opening, the hydrostatic pressure was logically removed.

2.2 Continuum formulation

The continuum field equations follow a Lagrangian formulation accounting for finite kinematics, inertia, and constitutive behavior. The formulation very closely follows the one given by Radovitzky and Cuitiño in 2003 [26].

We select the configuration $B_0 \subset \mathbb{R}^d$ of the body at time t_0 as the reference configuration. The coordinates $\mathbf{X}$ of points in B_0 are used to identify material particles throughout the motion. The motion of the body is described by the deformation mapping

$$\mathbf{x} = \varphi(\mathbf{X}, t), \qquad \mathbf{X} \in B_0 \tag{2.1}$$

Thus, $\mathbf{x}$ is the position of material particle $\mathbf{X}$ at time t. We shall denote by B_t the deformed configuration of the body at time t. The material velocity and acceleration fields follow from (2.1) as $\dot{\varphi}(\mathbf{X}, t)$ and $\ddot{\varphi}(\mathbf{X}, t)$, $\mathbf{X} \in B_0$, respectively, where a superposed $\dot{()}$ denotes partial differentiation with respect to time at fixed $\mathbf{X}$. The local deformation of an infinitesimal material neighborhood is described by the deformation gradient

$$\mathbf{F} = \nabla_0 \varphi(\mathbf{X}, t), \qquad \mathbf{X} \in B_0 \tag{2.2}$$

where ∇_0 denotes the material gradient of a function defined over B_0. Thus, the components of $\nabla_0 f$ are the partial derivatives of f with respect to $\mathbf{X}$. The scalar function

$$J = \det\big(\mathbf{F}(\mathbf{X}, t)\big) \tag{2.3}$$

is the Jacobian of the deformation, and measures the ratio of the deformed to undeformed volume of an infinitesimal material neighborhood. The local form of linear momentum balance is

$$\rho_0 \ddot{\varphi} - \nabla_0 \cdot \mathbf{P} = \rho_0 \mathbf{B}, \qquad \text{in } B_0 \tag{2.4}$$

where ρ_0 is the mass density in the reference configuration, $\mathbf{B}(\mathbf{X}, t)$ are the body forces per unit mass, and $\mathbf{P}(\mathbf{X}, t)$ is the first Piola-Kirchhoff stress tensor. The Cauchy stress tensor follows from $\mathbf{P}$ through the relation

$$\sigma = J^{-1}\mathbf{P}\mathbf{F}^T \tag{2.5}$$

The formulation of the initial boundary-value problem requires the specification of appropriate boundary conditions:

$$\varphi = \bar{\varphi}, \qquad \text{on } \partial B_{01} \tag{2.6}$$

where $\bar{\varphi}(\mathbf{X}, t)$ is the prescribed deformation mapping on the displacement boundary ∂B_{01},

$$\mathbf{P} \cdot \mathbf{N} = \bar{\mathbf{T}}, \qquad \text{on } \partial B_{02} \tag{2.7}$$

where $\bar{\mathbf{T}}(\mathbf{X}, t)$ are the prescribed tractions on the traction boundary ∂B_{02} and $\mathbf{N}$ is the unit outward normal, and initial conditions:

$$\varphi(\mathbf{X}, 0) = \varphi_0(\mathbf{X}) \tag{2.8}$$

$$\dot{\varphi}(\mathbf{X}, 0) = \dot{\varphi}_0(\mathbf{X}) \tag{2.9}$$

It must be emphasized that these boundary conditions are uniquely applied to the "outer boundaries" (i.e., the boundaries of the grain that are not in contact with another grain). The grain boundaries are modeled by the mean of other elements.

These other elements, called "interface elements", are composed of twelve nodes: 6 corner nodes and 6 mid-nodes (see Figure 2-2). This method closely follows the cohesive element approach to fracture proposed by Ortiz *et al.* [19].

By noting (s_1, s_2), the natural coordinates of the interface element midsurface[1] (on two consecutive edges of the midsurface), $N_a(s_1, s_2), a \in [1, 6]$ represent the standard shape functions of each of the nodes of a surface element. Between two surfaces of

[1]By numbering the nodes of a facet 1-4-2-5-3-6 going from one node to the next node (so going from corner node to mid-node or the contrary) around the triangle (See Figure 2-2)

adjacent tetrahedra, the coordinates of midsurface points are then defined by

$$\mathbf{x}(\mathbf{s}) = \sum_{a=1}^{6} \bar{\mathbf{x}}_a N_a(\mathbf{s}) \tag{2.10}$$

where

$$\bar{\mathbf{x}}_a = \frac{1}{2}(\mathbf{x}_a^+ + \mathbf{x}_a^-) \tag{2.11}$$

and $\mathbf{x}_a^{\pm}, a \in [1,6]$ are the coordinates of the upper surface nodes (subscript "+") and lower surface nodes (subscript "-") in the deformed configuration. The tangent basis vectors are then defined as

$$\mathbf{a}_\alpha(\mathbf{s}) = \mathbf{x}_{,\alpha}(\mathbf{s}) = \sum_{a=1}^{6} \bar{\mathbf{x}}_a N_{a,\alpha}(\mathbf{s}) \tag{2.12}$$

where $\alpha \in \{1,2\}$ represent the differentiation in the α-direction. The unit normal to the mid-surface can be expressed as

$$\mathbf{n} = \frac{\mathbf{a}_1 \times \mathbf{a}_2}{\|\mathbf{a}_1 \times \mathbf{a}_2\|} \tag{2.13}$$

And, by defining

$$[\![\mathbf{x}_a]\!] = \mathbf{x}_a^+ - \mathbf{x}_a^- \tag{2.14}$$

the opening displacement vector in the deformed configuration can then be written

$$\boldsymbol{\delta}(\mathbf{s}) = \sum_{a=1}^{6} [\![\mathbf{x}_a]\!] N_a(\mathbf{s}) \tag{2.15}$$

For convenience, the vector base $(\mathbf{a}_1, \mathbf{a}_2, \mathbf{n})$ is orthonormalized as follows:

$$\begin{cases} \mathbf{n}_1 = \frac{\mathbf{a}_1}{\|\mathbf{a}_1\|} \\ \mathbf{n}_2 = \mathbf{n} \times \mathbf{n}_1 \\ \mathbf{n}_3 = \mathbf{n} \end{cases} \tag{2.16}$$

The following quantities (respectively sliding of the upper element with respect to the lower one in directions $\mathbf{n}_1$ and $\mathbf{n}_2$ and opening) can be defined:

$$\begin{cases} \delta l_1 = \boldsymbol{\delta}.\mathbf{n}_1 \\ \delta l_2 = \boldsymbol{\delta}.\mathbf{n}_2 \\ \delta l_3 = \boldsymbol{\delta}.\mathbf{n}_3 \end{cases} \tag{2.17}$$

By inserting these interface elements in the meshing, no physical width is given to them, in other words, they are infinitely thin. Consequently, the question of how to define the strain corresponding to the opening in the direction normal to the grain boundary arises[2]. The same problem will occur when considering the shearing of the element defining the sliding of the two grains. However, as stated by Chokshi *et al.* [9], the grain boundary of a copper nanocrystal is known to be approximatively equal to 1 nm; therefore, fixing the grain boundary width (δ_{gb}) to 1 nm will avoid any problem. We can then define, the opening as following:

$$\epsilon_{33} = \frac{\delta l_3}{\delta_{gb}} \tag{2.18}$$

where δ_{gb}=1 nm. In agreement with what was done with the opening, the sliding can now be defined (see Figure 2-3):

$$\epsilon_{i3} = \epsilon_{3i} = \frac{\delta l_i}{2\delta_{gb}} \tag{2.19}$$

where i$\in\{1,2\}$

2.3 Constitutive model of the grains' bulk

The total deformation of a crystal is the result of two main mechanisms: dislocation motion within the active slip systems and lattice distortion. For most applications

[2]This is simply equivalent to dividing by zero

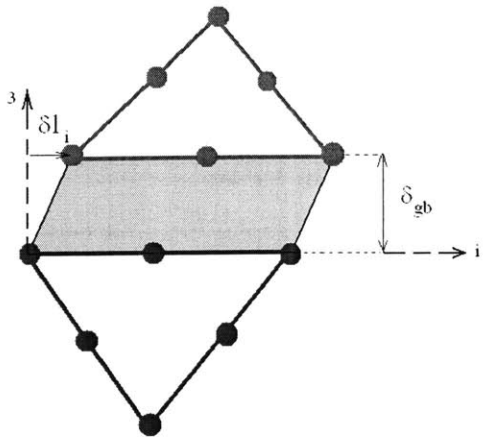

Figure 2-3: Sheared interface element in the "i"-direction where i∈{1,2}; ($\mathbf{n}_1$,$\mathbf{n}_2$) defining a basis of the grain boundary and $\mathbf{n}_3$ being the normal to the grain boundary.

involving metals, a linear (but anisotropic) relation between the Piola-Kirchhoff stress and the elastic lagrangean strain $\bar{\mathbf{E}} = (\bar{\mathbf{C}} - \mathbf{I})/2$ with $\bar{\mathbf{C}} = \mathbf{F}^T\mathbf{F}$ ($\mathbf{F}$ being the deformation gradient) can be assumed without much loss of generality. Higher-order moduli are given by Teodosiu [27].

The second step would be to complete the elastic step by taking an FCC (Face Centered Cubic) plastic formulation, i.e., to add a plastic step to the previous elastic description. But as has been pointed out by Schiøtz [11, 14, 16] in MD or Jiang and Weng [22] with their composite model, it seems that intragrain plasticity is negligible. Indeed, after a 10% stretching simulation of a 100,000 atoms copper cube, very little plasticity was observed as can be seen with the weak amount of dislocations (red atoms) in Figure 2-4. Similarly, Jiang and Weng ran two sets of tensile simulations, one with elastic grains and the other one with plastic grains. After a certain threshold in the size of the grains, yield stresses are observed to be the same for both elastic and plastic grains (See Figure 2-5). This threshold corresponds exactly to the break/transition between direct and reverse HP effect. These two results seem to converge towards the same conclusion; as was already stated, it seems difficult for dislocations pile-ups to occur in very small grains, and simulations clearly go into this direction. Consequently, the consideration of anisotropic elastic grains seems to

be a good approximation at the nanoscale level.

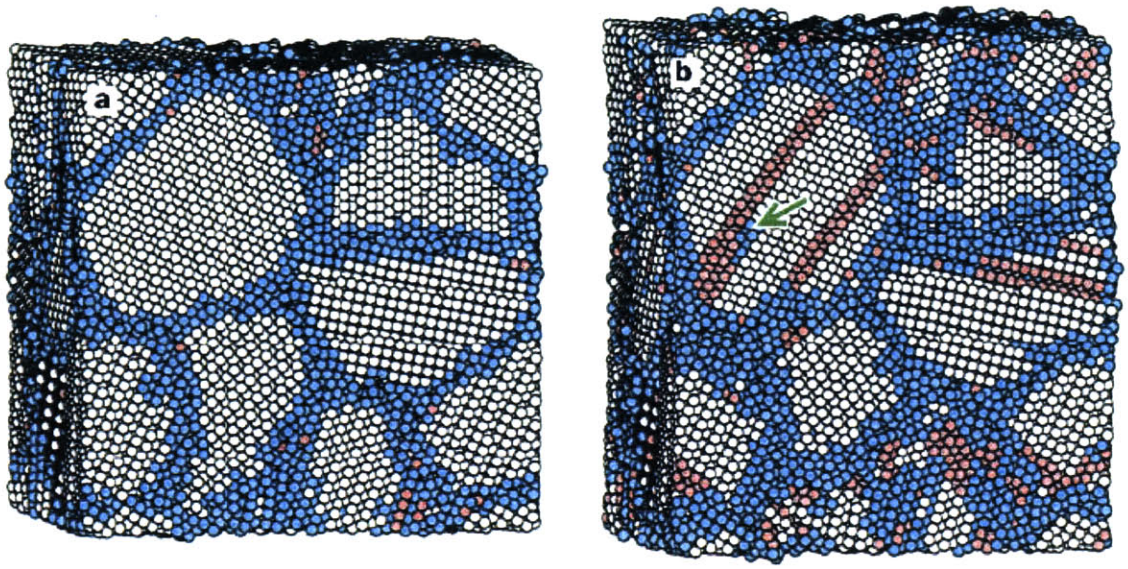

Figure 2-4: Before (a) and after (b) a 10% tensile test on a $5.2nm$ grain copper specimen (16 grains, 100,000 atoms) using Molecular Dynamics (Schiøtz *et al.* 1998). The white atoms correspond to the FCC grains' atoms, the blue ones to the GB's atoms and finally the red ones, to the intragrain dislocations.

Obviously, if further precision is required, a plastic model can be used. Nevertheless, anisotropic elasticity was chosen as a first good approximation. The corresponding parameters for FCC copper are given in Table 2.1.

Table 2.1: Cubic elastic constants and mass density used in calculations for anisotropic elastic FCC Copper grains

Mass Density (kg/m^3)	8000
C_{11} (Pa)	168.4e+09
C_{12} (Pa)	121.4e+09
C_{44} (Pa)	75.4e+09

The grain boundary model has to be created keeping in mind the restrictions and requirements given in the previous section.

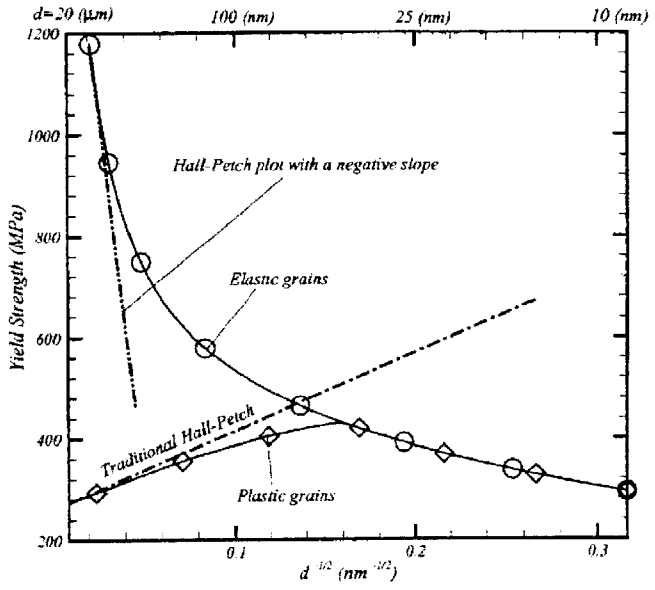

Figure 2-5: Comparison elastic/plastic grains for a nanocrystal tensile simulation of a composite model of Cu (B. Jiang and G.J. Weng, 2003)

2.4 Constitutive model of the grain boundary

By its nature, the grain boundary constitutive framework is intrinsically different from the grain's bulk one. Firstly, the model must be carefully designed not to allow any "negative opening", i.e. overlapping of two grains. Consequently, as soon as δl_3 becomes negative, a high elastic factor (called "interface parameter") is used to counter this overlapping. Otherwise the 1D plastic law is used.

The law described here is a typical small deformation rate-dependent isotropic plasticity law with combined isotropic and kinematic hardening. We define here the set of following "input/output" variables:

$$\begin{cases} \boldsymbol{\epsilon}, & \text{Initial total strain tensor;} \\ \boldsymbol{\epsilon^e}, & \text{Elastic strain tensor;} \\ \mathbf{C}, & \text{Deviatoric total strain tensor;} \\ \boldsymbol{C^e}, & \text{Deviatoric elastic strain tensor;} \\ \mathbf{s}, & \text{Cauchy stress tensor;} \\ W, & \text{Free energy.} \end{cases} \tag{2.20}$$

to which, we add the internal variables:

$$\begin{cases} \boldsymbol{\epsilon^p}, & \text{Plastic strain tensor;} \\ \epsilon^p_{eq}, & \text{Equivalent plastic strain;} \\ \boldsymbol{\sigma_{back}}, & \text{Back stress tensor;} \\ \sigma_y, & \text{Yield stress.} \end{cases} \tag{2.21}$$

These variables constitute a set of output and input to the plasticity law. The strain is related to its plastic and elastic part by the simple additive relation:

$$\boldsymbol{\epsilon} = \boldsymbol{\epsilon^p} + \boldsymbol{\epsilon^e} \tag{2.22}$$

where $\boldsymbol{\epsilon}$ has already been defined in the relations 2.19 and 2.18. The free energy relation is then given by

$$W = G|\boldsymbol{C^e}|^2 + \frac{1}{2}K(tr\boldsymbol{\epsilon}^e)^2 + W_{back} \tag{2.23}$$

where G and K are respectively the elastic shear and bulk moduli and W_{back} is the part of the free energy brought by the back stress $\boldsymbol{\sigma_{back}}$.

By derivation, the equation for the stress is then given by:

$$\mathbf{s} = 2G\boldsymbol{C^e} + K(tr\boldsymbol{\epsilon}^e)\mathbf{I} \tag{2.24}$$

The Von Mises stress is defined as a function of the Cauchy stress and the back stress:

$$\sigma_{eq} = \sqrt{\frac{3}{2}(s_{ij} - \sigma_{back\ ij})(s_{ij} - \sigma_{back\ ij})} \tag{2.25}$$

and the evolution equation for ϵ^p are then given by:

$$\dot{\boldsymbol{\epsilon^p}} = \frac{3}{2}\dot{\epsilon^p_{eq}}\mathbf{t} \tag{2.26}$$

with the flow direction $\mathbf{t}$ defined by:

$$\mathrm{t} = \frac{\mathbf{s} - \boldsymbol{\sigma_{back}}}{\sigma_{eq}} \tag{2.27}$$

submitted to the following yield condition:

$$\begin{cases} \epsilon^p_{eq} = 0, & \text{if } f = \sigma_{eq} - \sigma_y \leq 0 \\ \epsilon^p_{eq} \text{ verifying: } \begin{cases} \dot{\mathbf{s}} = 3G\dot{\epsilon^p_{eq}}\mathbf{t} \\ \sigma_{eq} = \sigma_0 \left(1 + (1-\beta)\frac{\epsilon^p_{eq}}{\epsilon_0}\right)^n \left(1 + \frac{\dot{\epsilon^p_{eq}}}{\dot{\epsilon_0}}\right)^m \end{cases}, & \text{if } f = \sigma_{eq} - \sigma_y > 0 \end{cases} \tag{2.28}$$

where ϵ_0, $\dot{\epsilon_0}$, m, n, σ_0 and β are fixed parameters and where the evolution equation of the back stress is given by:

$$\dot{\boldsymbol{\sigma_{back}}} = \frac{d}{dt}\left[\sigma_0\beta\left(1 + \frac{\epsilon^p_{eq}}{\epsilon_0}\right)^n\right]\mathbf{t} \tag{2.29}$$

Finally the new internal variables being solved and updated and $\mathbf{s}$ being found, the hydrostatic pressure $K(tr\boldsymbol{\epsilon})\mathbf{I}$ still needs to be added in order to obtain the final Cauchy stress. The resolution of this system of equations by Newton-Raphson iterations will give the deviatoric stresses $\mathbf{s}$ both for sliding and opening in *two different and independent* calculations respectively in 2D and in 1D (with K=0 for 1D). Solving such a system with Newton-Raphson iterations is simply done by checking the Yield condition in Equation 2.28 after a trial elastic step $\boldsymbol{s_{trial}} = 2G(\mathbf{C} - \boldsymbol{\epsilon^p})$. If the yield condition is satisfied, the plastic step is avoided, if not, the equations are solved for ϵ^p_{eq} with Newton-Raphson; then the internal variables are updated and the Cauchy

Stress is calculated.

Finally, the nodal forces can be computed from the individual opening and sliding tractions per unit area by

$$f_{ia}^{\pm} = \mp \int_{S_0} t_i N_a dS_0 \tag{2.30}$$

where S_0 is the undeformed reference surface, i, the direction, a, the number of the node and where the traction is defined as following:

$$\mathbf{t} = s_{13}^{sliding}\mathbf{n}_1 + s_{23}^{sliding}\mathbf{n}_2 + s_{33}^{opening}\mathbf{n}_3 \tag{2.31}$$

As can be seen, the plastic grain boundary model presents a full set of parameters, featuring back stress, hardening and rate dependency. This allows a lot of freedom in the way the calibration of the model can be done. While such a number of parameters allows a lot of precision in the calibration, it also drastically increases the complexity of the model because of the number of features. Naturally, some simplifications during the calibration may have to be done.

2.5 Numerical formulation

The preceding field equations may be rendered into a form suitable for computation by a combination of a time discretization of the momentum and constitutive equations and a finite-element discretization of the reference configuration of the solid. Some key aspects of the particular approach adopted here are summarized next for completeness and later reference. More detailed accounts may be found elsewhere [28].

We envision an incremental solution procedure aimed at sampling the solution at discrete times $t_0, \ldots, t_n, t_{n+1} = t_n + \triangle t, \ldots$. The linear-momentum balance equation (2.4) is discretized in time by recourse to the second-order accurate explicit central-

difference time-stepping algorithm:

$$\varphi_{n+1} = \varphi_n + \triangle t\, \dot{\varphi}_n + \frac{\triangle t^2}{2} \ddot{\varphi}_n \tag{2.32}$$

$$\dot{\varphi}_{n+1} = \dot{\varphi}_n + \triangle t\, \ddot{\varphi}_n \tag{2.33}$$

$$\rho_0 \ddot{\varphi}_{n+1} - \nabla_0 \cdot \mathbf{P}_{n+1} = \rho_0 \mathbf{B}_{n+1} \tag{2.34}$$

where the subscript n refers to time t_n, and $\dot{\varphi}_n$ and $\ddot{\varphi}_n$ are the material velocity and acceleration fields.

Details on the constitutive variational update algorithms which allow to compute the stresses at time t^{n+1} are given elsewhere [28, 29].

A finite-element discretization of the linear momentum balance equation may be based on the weak form

$$\begin{gathered} \int_{B_0} \rho_0 \ddot{\varphi}_{n+1} \cdot \mathbf{v}\, d\Omega + \int_{B_0} \mathbf{P}_{n+1} : \nabla_0 \mathbf{v}\, d\Omega = \\ \int_{\partial B_{02}} \bar{\mathbf{T}} \cdot \mathbf{v}\, dS + \int_{B_0} \rho_0 \mathbf{B}_{n+1} \cdot \mathbf{v}\, d\Omega,\ \forall \mathbf{v} \in V \end{gathered} \tag{2.35}$$

where V is the space of admissible displacements, i. e., such incremental displacements, or, alternatively, velocities, that satisfy the essential boundary conditions (2.6) in the sense of traces. This weak statement is also known as the principle of virtual work. We consider finite-element interpolations of the form

$$\varphi_h(\mathbf{X}) = \sum_{a=1}^{N} \mathbf{x}_a N_a(\mathbf{X}) \tag{2.36}$$

where φ_h is the deformation mapping interpolant; N_a are the displacement shape functions respectively; the sum on a ranges over the N nodes in the mesh, whereas the sum on e ranges over the E elements in the mesh. The displacement shape functions N_a must be conforming. In calculations we employ standard quadratic ten-noded tetrahedra [30]). The interpolation of the vast number of internal variables in the crystal plasticity models can be chosen to be piecewise polynomials..

To render these formulation in a form suitable for finite element discretization, we

recast the linear momentum balance equation in weak form:

$$\int_{B_0} \Big[\mathbf{P} : \nabla_0 \eta - \rho_0 \big(\mathbf{B} - \ddot{\varphi} \big) \Big] dV_0 - \int_{\partial B_{02}} \mathbf{T} \cdot \eta dS_0 = 0 \tag{2.37}$$

where the test functions η satisfy the homogeneous essential boundary conditions $\eta = 0$ on ∂B_{01}.

Chapter 3

Application to the prediction of size effects in nanocrystalline copper

In this final chapter, two kinds of published results for copper will be considered: molecular dynamics' and experimental results. For both cases, the model developed in this work will be calibrated and a comparison will be done between its results and the published data. Finally, the influence of the grain boundary yield stresses and the rate-dependency coefficient will be studied and discussed.

3.1 Model calibration to experiments

As can be seen in Figure A-1, no general trend can be found between all the different sets of data for copper. Some results are similar and in good agreement with each other (e.g. Jiang and Weng's with Sanders'), some others (the whole set of MD simulations) behave as an independent group and do not agree with any experimental result, and in the middle, some are simply not following any trend.

As has already been discussed in the Introduction, the discrepancy between these results and the experimental results can be attributed to a lot of different phenomena, from high strain rate effects to the absence of defaults in the lattices. Consequently,

calibrating the model on the molecular dynamics' results and on Sanders' will require a different approach.

In this section, one set of experimental results will be studied. Two results from Sanders [20, 21, 22] are given in Figure A-1 (and later in this chapter in Figure 3-4); one is fitted well by Jiang and Weng's model [22] for the direct HP part of the curve, and the other clearly shows the transition and the beginning of the reverse HP effect. These three curves agree in good proportion and can be taken as a set of data that our model could capture[1].

One of Sanders' stress-strain curves for a tensile test of a 26 nm grain size specimen [20] will be taken as a reference; the model will then be fitted to this result by considering a 4x4x4 100 nm specimen (consequently for a grain size of approximatively 25 nm) and stretching it until 1% of strain. Finally, after this calibration, the reverse HP effect will be studied.

An initial set of values for the parameters was arbitrarily chosen as a basis for the calibrations (See Table 3.1). The yield stresses and Young's moduli were taken from the bulk values, with the help of Jiang and Weng's parameters [22]. Both hardness and rate-dependency have been taken to their limits, and back stress features have not been taken into account (β=0).[2]

One of the distinctive features of the experiments compared to MD simulations is the very low strain-rate. As a consequence, calibrating the model on Sanders' results can be done considering rate-independency and keeping the rate-dependency power coefficient m very low (1e-03). With this value being fixed, the yield stresses were varied in order to match the 25 nm grain size curve to Sanders' curve. A final value of 410 MPa was found to provide good agreement (see Figure 3-1).

The values of the parameters and specific information concerning the simulation

[1]It should be emphasized though that Jiang and Weng's results are not experimental but correspond to a composite model fitted on Sanders' results

[2]The interface parameter has been chosen to be 100 times the Young's moduli and previous tests not given here have shown that for such a value, no overlapping of grains was occurring for pure compression

Table 3.1: Model parameters *before* calibration for Copper grain boundaries

Young's modulus (Pa)	108.0e+09
Poisson's ratio	0.33 / 0 (sliding / opening)
σ_0 (Pa)	145.0e+06
ϵ_0	1.0
$\dot{\epsilon_0}$ (s^{-1})	1.0
1/n	1000
1/m	1000
β	0
Interface Parameter (Pa)	108.0e+11

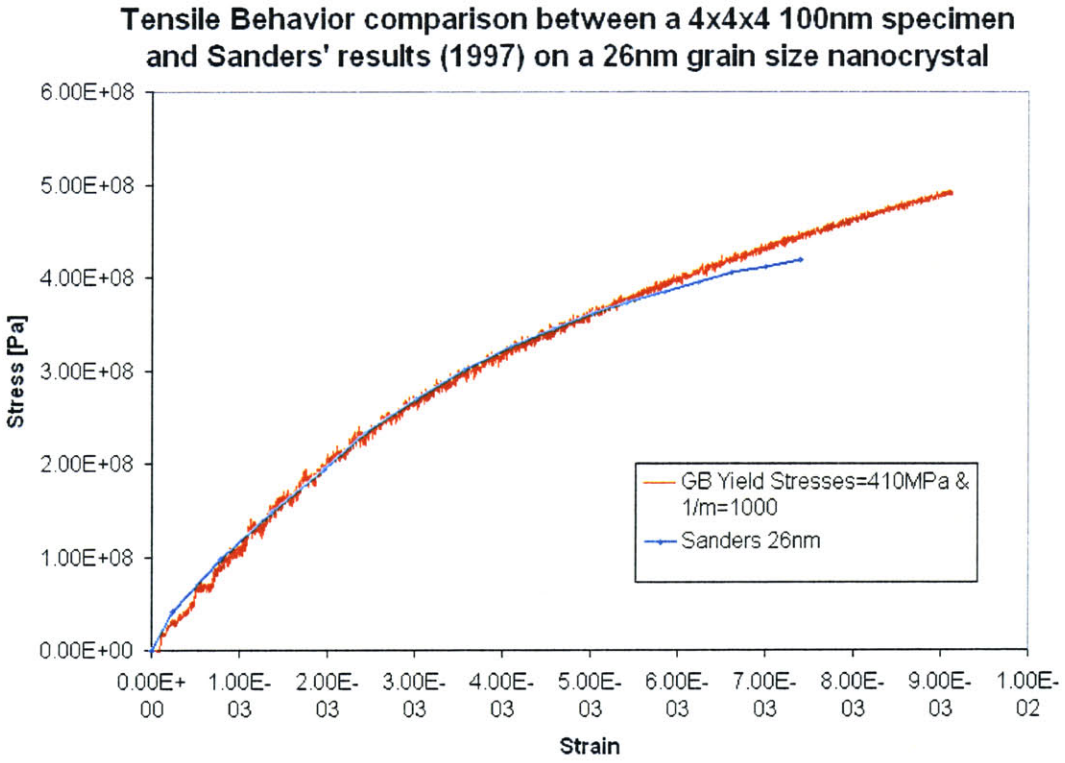

Figure 3-1: Fit of a 25 nm grain size tensile simulation on a 26 nm grain size tensile test done by Sanders (1997)[20]

can be found in Table 3.2. Adjusting other parameters would clearly allow a better fit of the curve, but, due to the significant differences between the published data, even a "perfect fit" of one experimental curve would be far from a representative result of the exact behavior. As such, there is no use for further calibration.

Table 3.2: Simulation and Model parameters *after* calibration on Sanders' results [20] for Copper grain boundaries

Cube's edge size (nm)	100
Speed of deformation (ms^{-1})	0.5
Strain rate	5e+06
Young's modulus (Pa)	108.0e+09
Poisson's ratio	0.33 / 0 (sliding / opening)
σ_0 (Pa)	410.0e+06
ϵ_0	1.0
$\dot{\epsilon_0}$ (s^{-1})	1.0
1/n	1000
1/m	1000 (rate independent)
β	0
Interface Parameter (Pa)	108.0e+11

The fit of our model to Sanders' curve allows a closer look at the grain size dependency to now be given.

This first set of simulations was done with nxnxn 100 nm cube where $n \in [3, 6]$ (see Figure 3-2). Consequently, as already explained in the previous chapter, the specimens respectively have 91, 189, 341 and 559 grains with a mean size of 33.33nm, 25 nm, 20 nm and 16.67 nm.[3] A speed of 0.5 m/s has been chosen as a balance between time of calculation (very small speeds imply tremendous computational time) and the necessity to reduce the dynamic oscillations with a small enough velocity. Knowing that a full grain is modeled by 192 tetrahedra (to which are added the cohesive elements) and that in a nxnxn specimen, there are 2xnxnxn full grains (if we assemble all the portions of grains together), these cubic specimens are respectively represented by 10368, 24576, 48000 and 82944 tetrahedra plus the cohesive elements at each grain boundary. The set of results is given in Figure 3-3.

[3]This "mean" size corresponds more exactly to the approximate diameter of the full grains

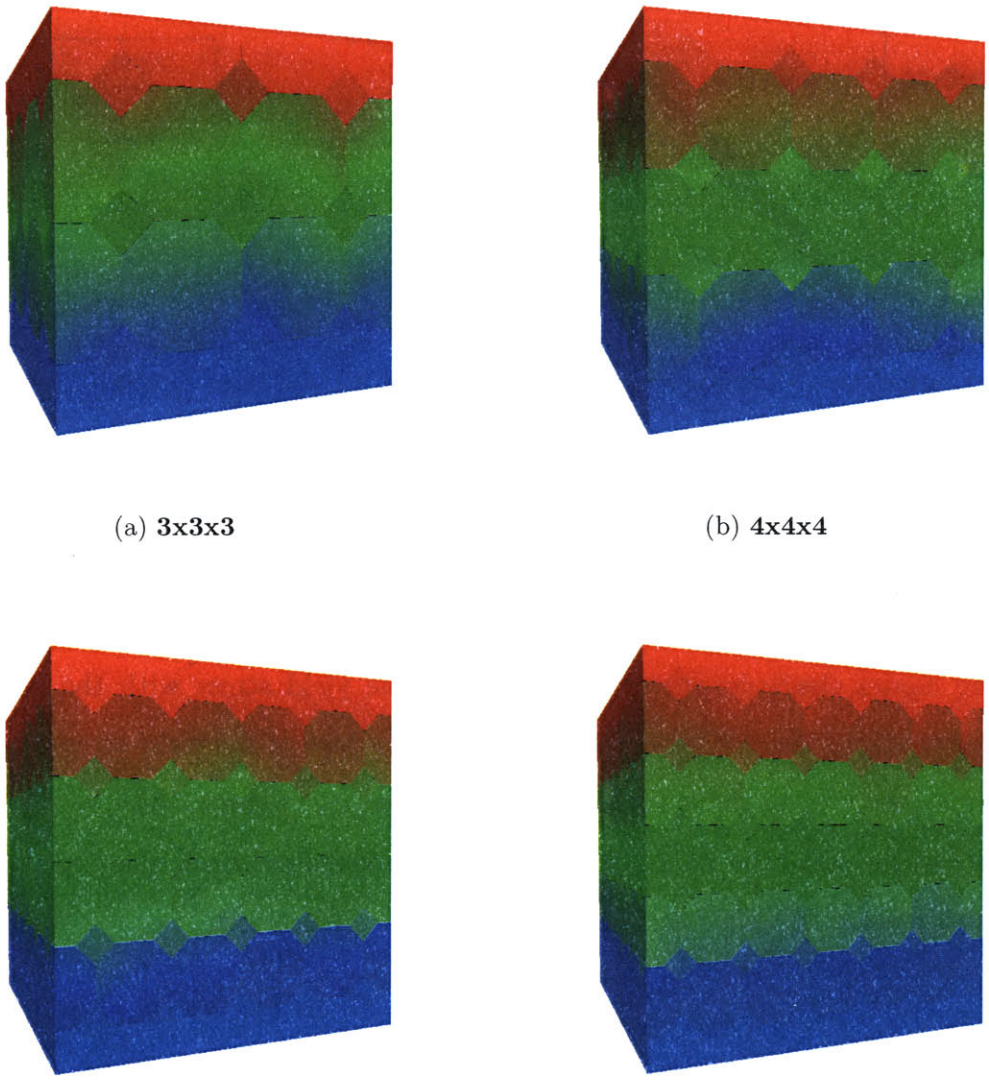

(a) **3x3x3**

(b) **4x4x4**

(c) **5x5x5**

(d) **6x6x6**

Figure 3-2: Displacement fields of 1% stretches of nxnxn 100 nm cube where $n \in [3, 6]$

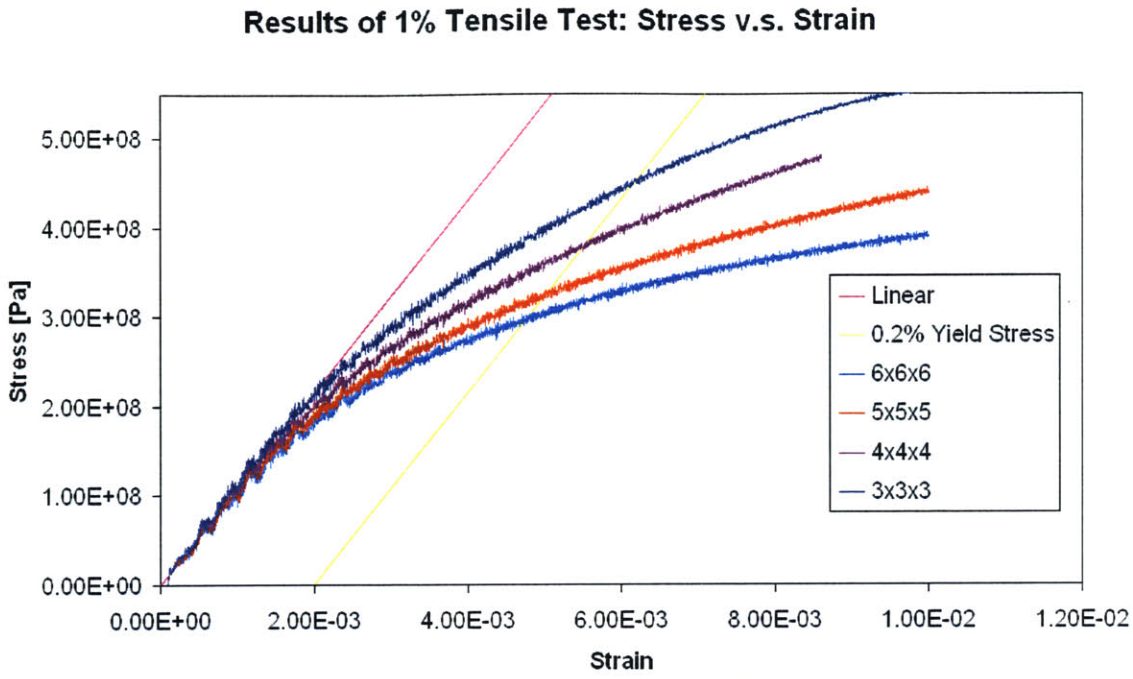

Figure 3-3: Set of simulation done for different grain size after calibration with Sanders' results [20]

The model clearly captures a decrease of the yield stress with the grain size. Moreover, taking the 0.2% yield stress criterion, a plot of the yield stress versus the inverse square root of the grain size can be plotted (see Figure 3-4).

As can be seen, the model follows in good agreement both the experimentally observed reverse HP effect and Jiang and Weng's prediction.

3.2 Comparison with molecular dynamics

In this second section, the attention will be focused on MD. As can be seen in Figure A-1, both slopes and values are in good agreement between the different sets of reverse HP effects, either for Schiøtz [11, 14, 16] or for Heino *et al.* [31].

The approach taken in this section is similar to the one taken in the previous section. Schiøtz' stress-strain curve for a tensile test on a specimen with a 6.56 nm mean grain size is chosen as a reference [11]. A 10% stretching test of a 3x3x3 20nm

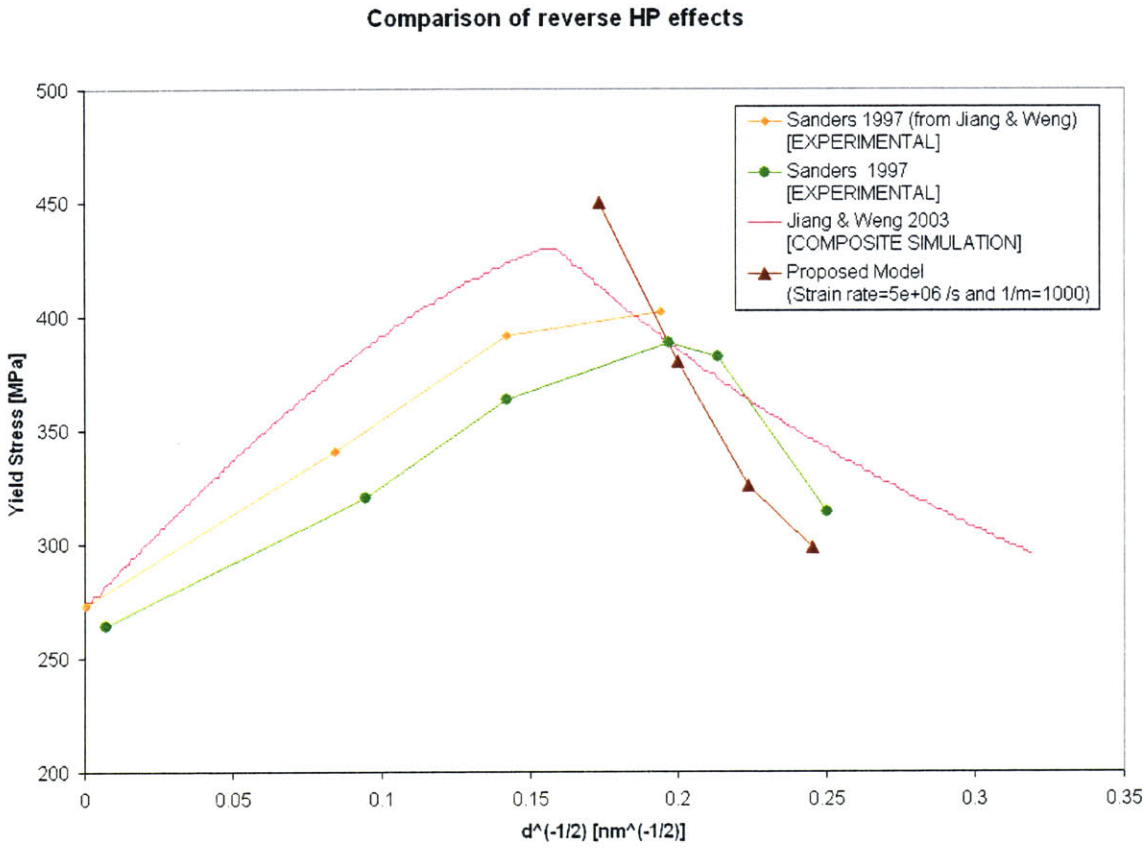

Figure 3-4: Comparison of the reverse HP effects between the calibrated model, Sanders' results and Jiang and Weng's [20, 21, 22]

specimen[4] is then considered. The parameters of the model are finally varied in order to fit Schiøtz' results, and the reverse HP effect of the model then calibrated is studied.

Having calibrated the model for Sanders' result and considering the discrepancies between the perfect lattices used in MD and the imperfect ones used in experiments, a first reflex would be to increase the yield stresses to match Schiøtz' result. Nevertheless, our model is rate-dependent and by increasing the power coefficient m (or decreasing 1/m) for a similar strain rate such as the ones used by Schiøtz in his MD calculations, our model will capture the specific feature of MD calculations concerning the strain rate. The idea here is then to take the previous calibrated model and compare it to Schiøtz' results by a minimum of change.

After a few preliminary tests, a good fit was found, with 1/m=11.32, keeping the yield stresses equal to 410MPa. Time convergence was checked and, because the model was this time rate-dependent, special care was given to the strain rate used by Schiøtz in 2003 [16] and the same was used for our simulation. All the parameters are given in Table 3.3. The fit to Schiøtz' curve is given in Figure 3-5.

Table 3.3: Simulation and Model parameters *after* calibration on Schiøtz' results [11] for Copper grain boundaries

Cube's edge size (nm)	20
Speed of deformation (ms^{-1})	10
Strain rate	5e+08
Young's modulus (Pa)	108.0e+09
Poisson's ratio	0.33 / 0 (sliding / opening)
σ_0 (Pa)	410.0e+06
ϵ_0	1.0
$\dot{\epsilon_0}$ (s^{-1})	1.0
1/n	1000
1/m	11.32 (rate dependent)
β	0
Interface Parameter (Pa)	108.0e+11

This fit is not only remarkable by its very good approximation but also by the fact that from Sanders' calibration, only the rate dependent power coefficient has

[4]The mean grain size is approximatively equal to 6.67nm

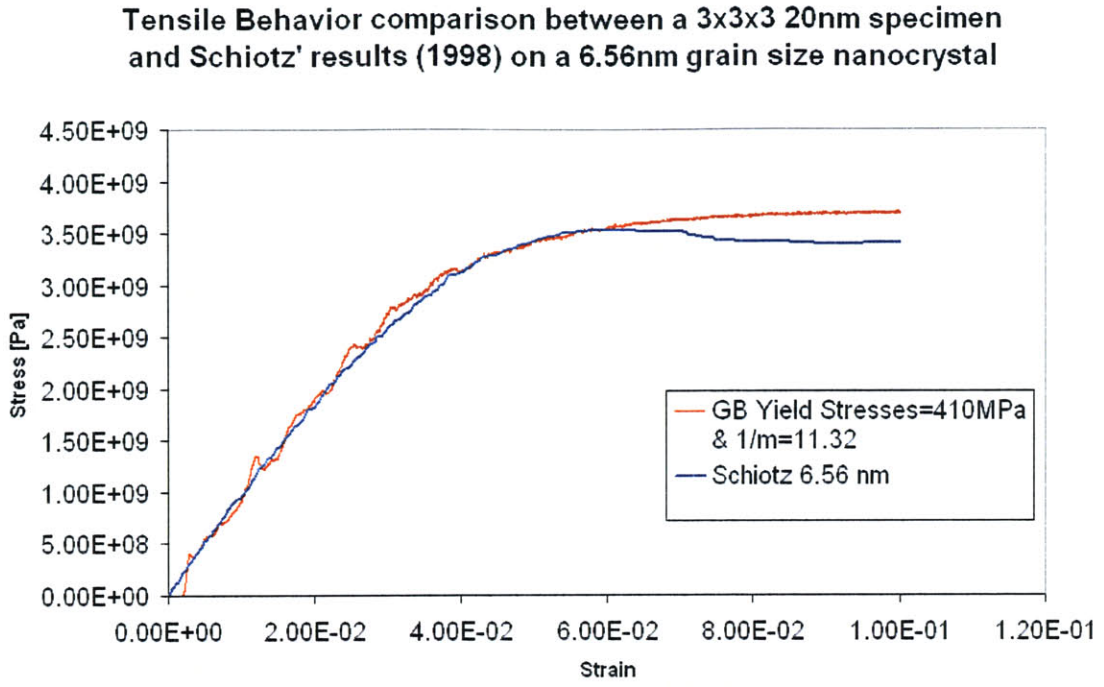

Figure 3-5: Fit of a 6.67 nm grain size tensile simulation on a 6.56 nm grain size tensile MD simulation done by Schiøtz (1998)[11]

been changed, making the difference between Sanders' results and Schiøtz' ones only a rate-dependency related discrepancy.

After setting up the model, a complete set of $nxnxn$ (where $n \in [2, 6]$) 20nm cube tensile simulations was done (see Figure 3-6). The mean grain size was consequently equal to 10nm, 6.67nm, 5nm, 4nm and 3.33nm in the different tests. Time convergence was checked, and the runs were done with the parameters chosen above (Table 3.3). The set of results is given in Figure 3-7. The Figure 3-8 gives the sliding and opening fields exclusively at the grain boundary. For each interface element, only one of the two facets is represented. As could have been foreseen, the opening is mainly concentrated at the grain boundaries normal to the deformation axis, and the sliding, at the grain boundaries in the other configurations except for the facets parallel to the deformation axis; those naturally do not slide because both facets of the interface elements are submitted to the same tensile deformation in their planes.

Schiøtz, in his publications, considered both the 0.2% yield stress and the flow

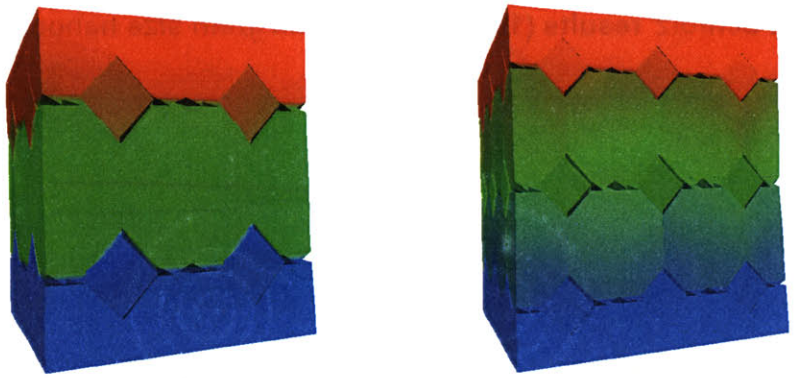

(a) **2x2x2**

(b) **3x3x3**

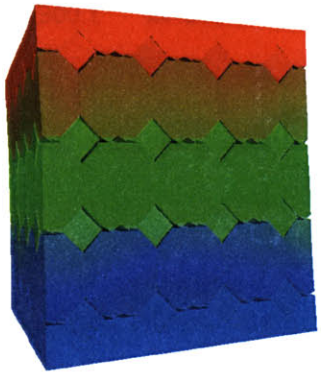

(c) **4x4x4**

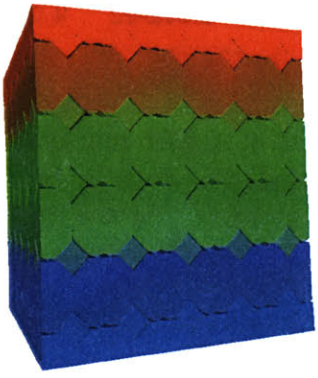

(d) **5x5x5**

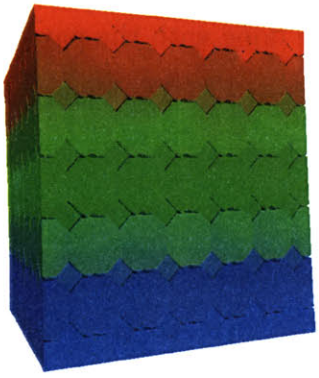

(e) **6x6x6**

Figure 3-6: Displacement fields of 10% stretches of nxnxn 20 nm cube where $n \in [2, 6]$

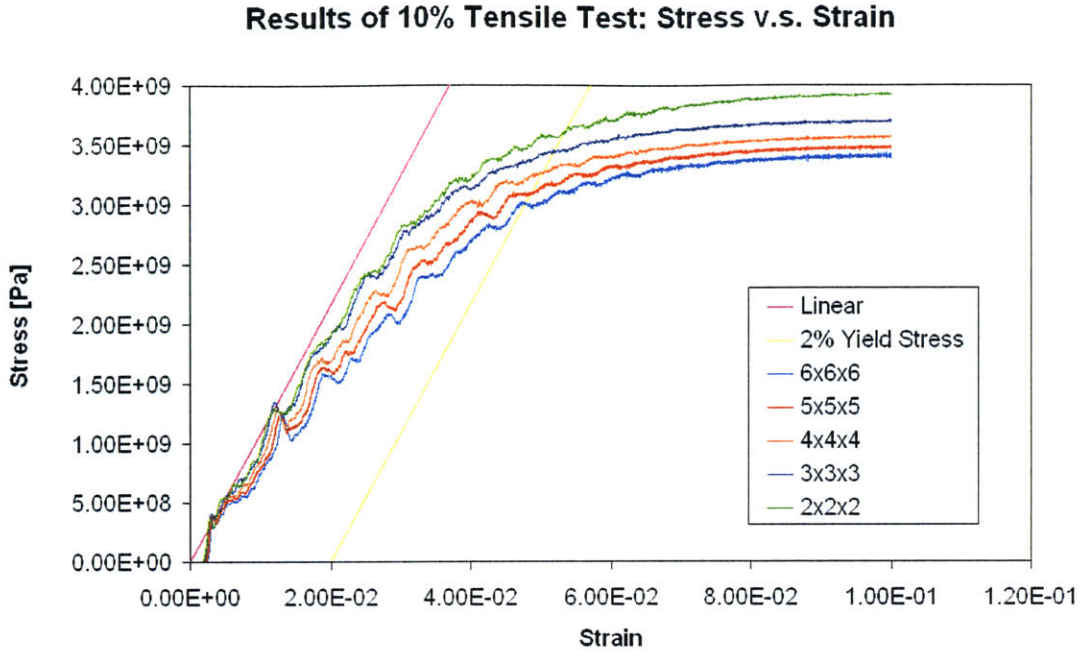

Figure 3-7: Set of simulation done for different grain size after calibration with Schiøtz' results [11]

stress criteria to plot the reverse HP effects [11, 14, 16]. Our approach being dynamics, the simulations naturally have small oscillations along the curves and taking a 0.2% yield stress criterion would not lead to a valuable criterion because of the "late" yield (as opposed to Sanders') and too many close oscillations between all the curves. Consequently, a 2% yield stress criterion was chosen.

A first look already confirms the same behavior as what we had in the previous section: a decrease of the yield stress with the size of the grain. Plotting the 2% yield stress (Figure 3-9) definitively confirms both the reverse HP effect, with a remarkably straight line, and good agreement with Schiøtz' 1998 results [11].

3.3 Discussion

In the last two sections, the same approach was taken: first, the model was fitted to a result (experimental and molecular dynamics) by considering one stress-strain

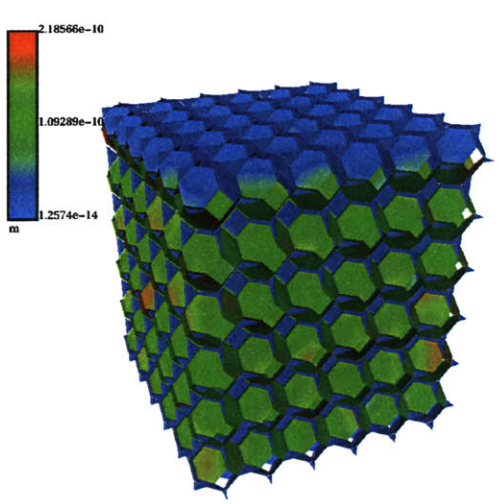

(a) **Sliding field**

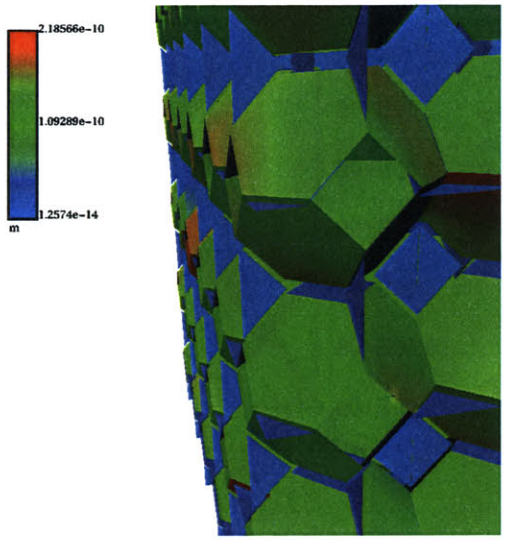

(b) **Sliding field after zoom**

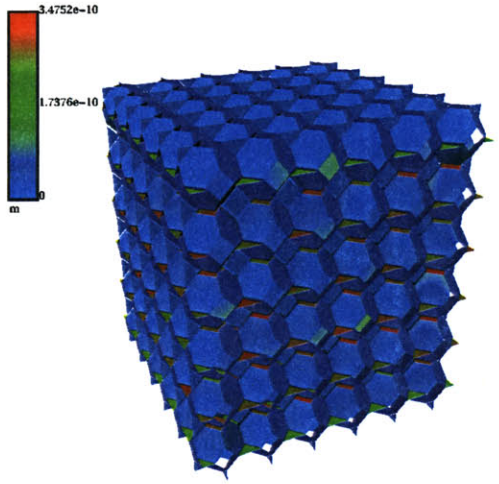

(c) **Opening field**

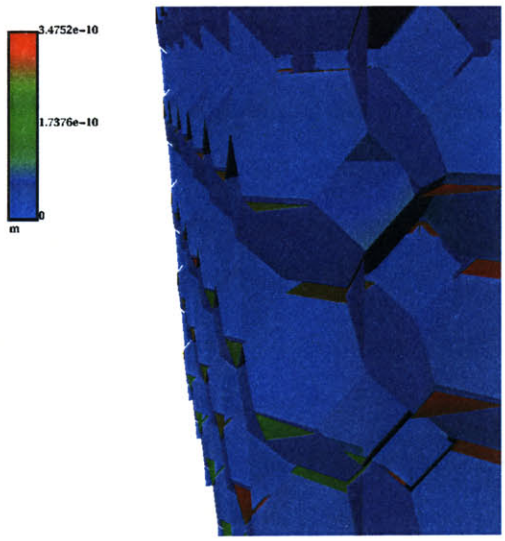

(d) **Opening field after zoom**

Figure 3-8: Sliding and opening fields at the GBs of a 10% stretch of 6x6x6 20 nm cube

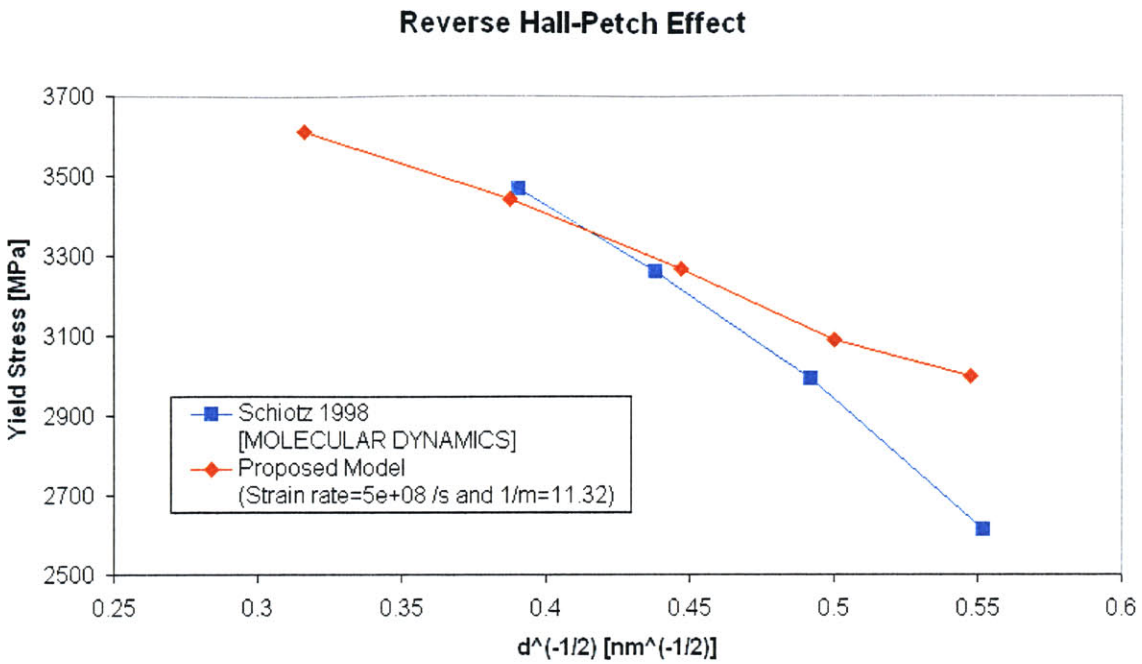

Figure 3-9: Comparison of the reverse HP effects between the calibrated model and Schiøtz' results

curve for a given grain size; then, the grain size was gradually decreased, and the yield stress as a function of the inverse square root of the grain size was plotted from the previous set of calculations. In both cases, a clear reverse HP effect was observed accordingly to the linear relation between the yield stress and the inverse square root of the size of the grains.

A few conclusions may be drawn from this work. First of all, our phenomenological model captures the plastic behavior in the deformation of a nanocrystal. Given that the grains are elastic, all the plasticity observed in the deformation can uniquely be attributed to grain boundary effects. These effects, namely grain boundary sliding accommodated by dissipative opening mechanism, closely follow both experimental and MD observations at the continuum level as can be seen in Figures 3-1 and 3-5.

Secondly, as shown in Figures 3-3 and 3-4, on the one hand, and Figures 3-7 and 3-9, on the other hand, the decrease of the grain size implies a decrease of the yield stress of the specimens. The reverse HP effect observed in both cases strongly follows the respective mimicked results: Schiøtz' [11] and Sanders' [21] (see Figure 3-10).

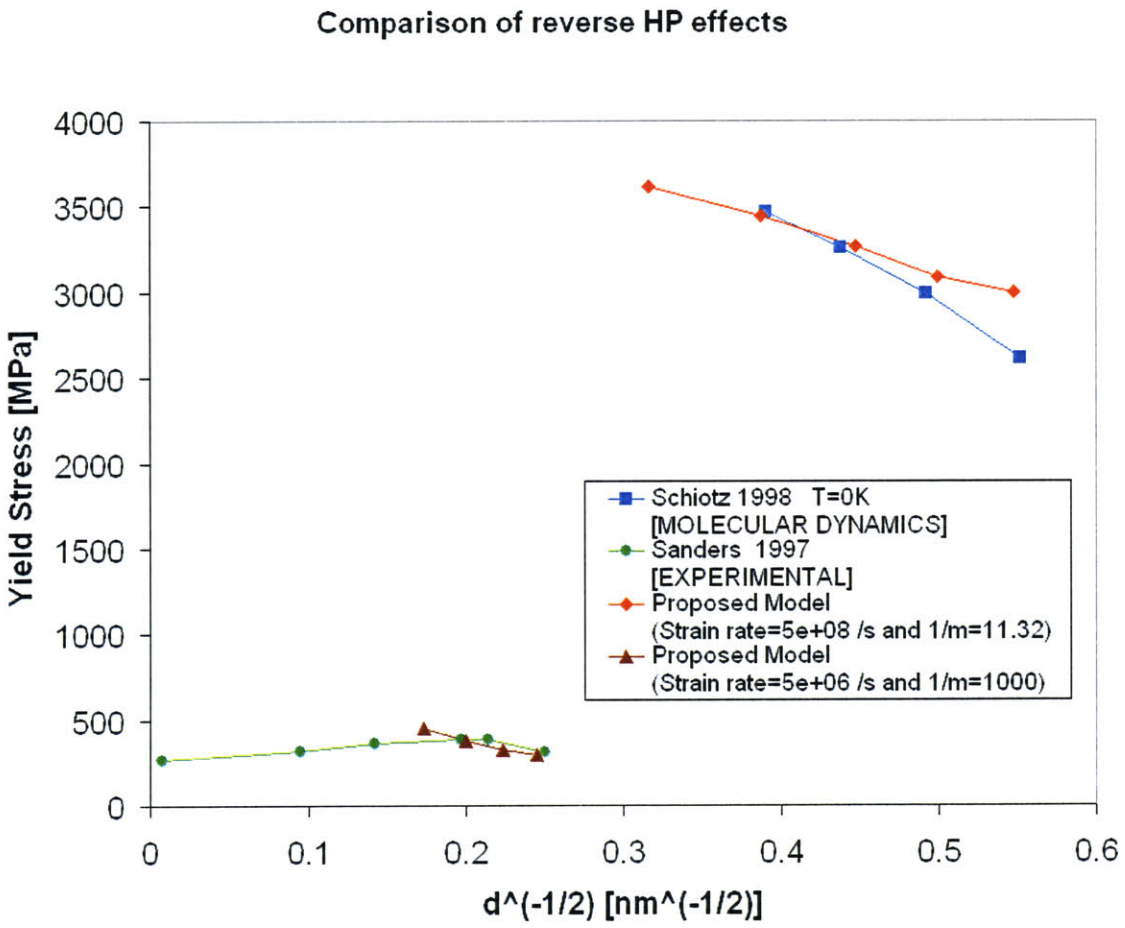

Figure 3-10: Comparison of the reverse HP effects between the calibrated models for Sanders and Schiøtz, Sanders' results and Schiøtz' results [21, 11]

Finally, one of the most noticeable facts is related to the match to the two results by the unique variation of the rate dependency power coefficient. It must be emphasized that, even though there are many reasons for this to happen and that a complete understanding of its causes and results has not been achieved yet, the continuum model created here clearly predicts that the difference between experimental and molecular dynamics results is due to the rate dependency of the two deformation processes.

Adding rate-dependent features to the model is definitely a way of "lowering" or "raising" the yield stress as a function of the strain rate. The differences in the values of yield stress between Schiøtz' results and Sanders' is approximatively a factor of 3 (with the 0.2% offset criterion for both). Instead of varying 1/m as we did, another approach would consist of keeping the same value for 1/m (taking the one in Table 3.3 for Schiøtz's calibration) but changing $\dot{\epsilon}$ in order to fit Sanders' results. We can then find an estimation of the speed that we would have to take for a good fit to Sanders' results, by taking a common set of parameters (namely here, a same "1/m", the other parameters being already the same). Let's define V_i, $\dot{\epsilon}_i$ and l_i for $i \in \{1, 2\}$ where these are respectively the speed of deformation, the strain rate and the length of the cube's edges for Schiøtz' ($i = 1$) and Sanders' fit ($i = 2$). In this case, we consequently choose $l_1 = 20nm$, $l_2 = 100nm$ and $V_1 = 10ms^{-1}$, implying, $\dot{\epsilon}_1 = 5\ 10^8 s^{-1}$. By considering Equation 2.28,

$$\sigma_y^1 \sim (\dot{\epsilon}_1)^m \sim \left(\frac{V_1}{l_1}\right)^m \tag{3.1}$$

$$\sigma_y^2 \sim (\dot{\epsilon}_2)^m \sim \left(\frac{V_2}{l_2}\right)^m \tag{3.2}$$

Consequently, by dividing these two relations,

$$\frac{\sigma_y^1}{\sigma_y^2} \sim \left(\frac{\dot{\epsilon}_1}{\dot{\epsilon}_2}\right)^m \sim \left(\frac{V_1}{l_1}\frac{l_2}{V_2}\right)^m \tag{3.3}$$

And by putting the known values,

$$3 \sim \left(\frac{10}{20\ 10^{-9}} \frac{100\ 10^{-9}}{V_2} \right)^{1/11.32} \Leftrightarrow V_2 \sim \frac{10\ 100\ 10^{-9}}{20\ 10^{-9}}\ 3^{-11.32} \sim 0.0002\ m/s \quad (3.4)$$

As a consequence, by taking $V_2 = 2\ 10^{-4} m/s$, the same parameters for the plasticity as for Schiøtz' comparison and a $100nm$ edge size cube, a good fit to Sanders' results is expected. Such a speed would clearly require a drastically long time of simulation and has not been done in the framework of this work but this short analysis proves that a good fit is also expected, giving a very low speed of deformation compatible with the quasi-static indentation process.

Chapter 4

Summary and conclusions

We developed a phenomenological model for grain boundary sliding in nanocrystals. An accommodation process, chosen here to be a dissipative opening mechanism, was added to this plastic sliding law in order to allow for sliding despite intrinsic problems arising from the definition of the grain boundary (for instance at triple points). Based on observations of different works [11, 14, 13, 16, 22], it is believed that very little intra-grain plasticity occurs during nanocrystalline deformation. As a consequence, anisotropic elasticity was chosen to define the behavior of the grains. Both continuum frameworks and constitutive laws have been set up for grain boundary and grains, accounting for what was previously done in published experiments', molecular dynamics' or other simulations' results, defining interface element at the grain boundary and characterizing the strains for these elements.

The model carefully set up was then calibrated on both Sanders' [20, 21] and Schiøtz' [11] results. For both results, a full set of common parameters was found, the only difference being in the strain rate dependency power coefficient "m". Whereas a rate independent limit (1/m=1000) was used for Sanders' fit, a strongly rate dependent framework (1/m=11.32) was taken for Schiøtz'. In both cases, a good fit to the stress-strain curves and to the reverse HP effect curves was observed. It bears emphasis that in spite of its phenomenological character and of leaving unmodeled potentially significant features affecting the behavior of grain boundaries such as the lattice misorientation and boundary angle, the model proposed succeeds in captur-

ing the main feature of the effective behavior afforded by atomistic descriptions at a much lower cost, i.e., without the need of tracking the evolution of individual atoms. However, no direct interpretation of this significant result can be given without care. It must be emphasized that many reasons not investigated in this work could be at the origin of this, but it has been seen that the model predicts a fit for both molecular dynamics and experiments by the unique variation of the strain rate dependency coefficient (or the strain rate itself as seen in the *Discussion* of the previous chapter); this result could then make the bridge between molecular dynamics and experiments.

Appendix A

Literature review

From the 1950s to now, many papers have been published either exclusively on the mechanism of grain boundary sliding or on more general aspects of polycrystal deformation (the former being naturally part of the latter). The goal of this review is to gather enough information to be able to analyze and set up some bases for the modeling of nanocrystalline deformation. Therefore, a complete study of the direct HP effect and other microcrystals is not entirely necessary (by comparison with the reverse HP effect and the nanocrystalline deformation). The need here is to understand the very essential principles of grain boundary sliding and to couple them with nanocrystals studies. It is in this spirit that the following sections will be reviewed: the different experiments done on nanocrystals, then some of the theories that have been more or less successfully associated with them, and finally the simulations, either in molecular dynamics, in FEM or with other models.

The review is conducted in a chronological fashion and the corresponding graphs are sorted by type of material. For each material, experimental, theoretical, and model results are given. For each graph, data are given under the form of a "σ_y v.s. $d^{-\frac{1}{2}}$" curve. Nevertheless, a lot of experimental data are given with hardness values (following some indentation process), but hardness is known to follow the direct and reverse HP relations the same way as in Equation 1.1, the only difference being that the proportional factor is approximatively three times the one associated to the yield stress [7] (for nanocrystals). However, the additive constant is not known.

Consequently, in order to be able to compare hardness and yield stress results, the values of hardness curves have been divided by three. The slopes are then made comparable but the reader should keep in mind that the exact position along the y-axis is not known (the curve is then subject to vertical translation). Lastly, the adapted hardness curves will be represented by dash lines, and the yield stress results, by solid lines except for results with no noticeable trend for which only symbols will be used; the simulation results will be plotted with thin symbols ($\times$, $+$, $\ast$ and $-$), the experimental, with bigger symbols, full for yield stress (■, ♦, ▲ and •) and hollow (□, ◊, △ and ○) for hardness, except for Jiang and Weng's results which is a continuous line.

A.1 Experimental work

The following section will not review all the experimental papers done on the *direct* HP effect in depth; only a few ones will be discussed. On the contrary, a closer look will be given to the *reverse* HP effect. On the graphs, the legend "A from B" means that the results are A's but have been taken in B's paper. Most given results are either tensile tests or indentation tests. Finally, the data have been taken with the help of the software DataThief®.

One of the first experimental discoveries concerning the nanocrystals was done by Chokshi *et al.* [9] in 1989. Their hardness measurements were done on copper and palladium (Figure A-1 and Figure A-2) and first exhibited a clear deviation from the HP relation (at this time, there was only one relation: the direct HP effect). Secondly, their measurements showed that the HP relation was still valid by taking the multiplicative constant as being negative. Chokshi associated this result to a drastic increase in grain-boundary diffusion, also called Coble creep (as opposed to Nabarro-Herring diffusion which is an intragrain diffusion) when the size of the grain would become very small.

Following these first results, experimental results of both the direct HP effect and reverse HP effect continued to be published. For the direct HP effect, the reader

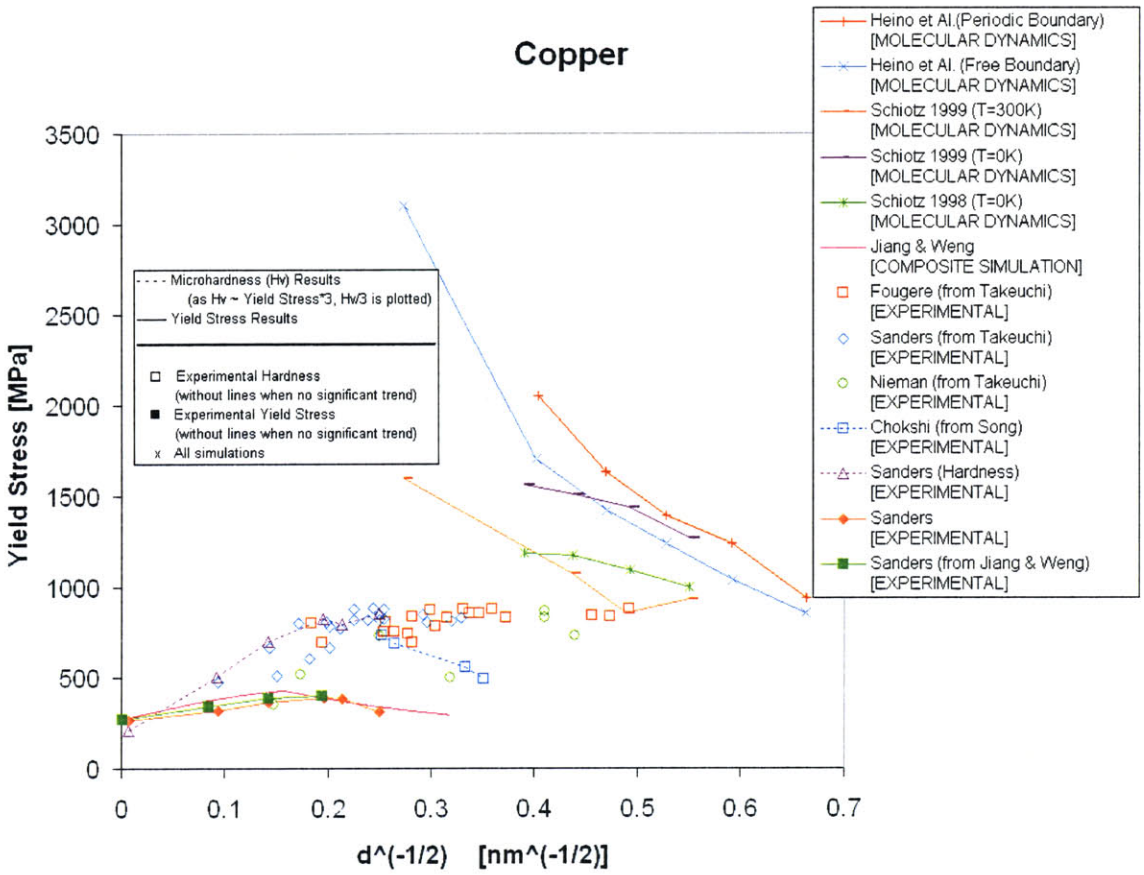

Figure A-1: Published results for the HP effects for copper

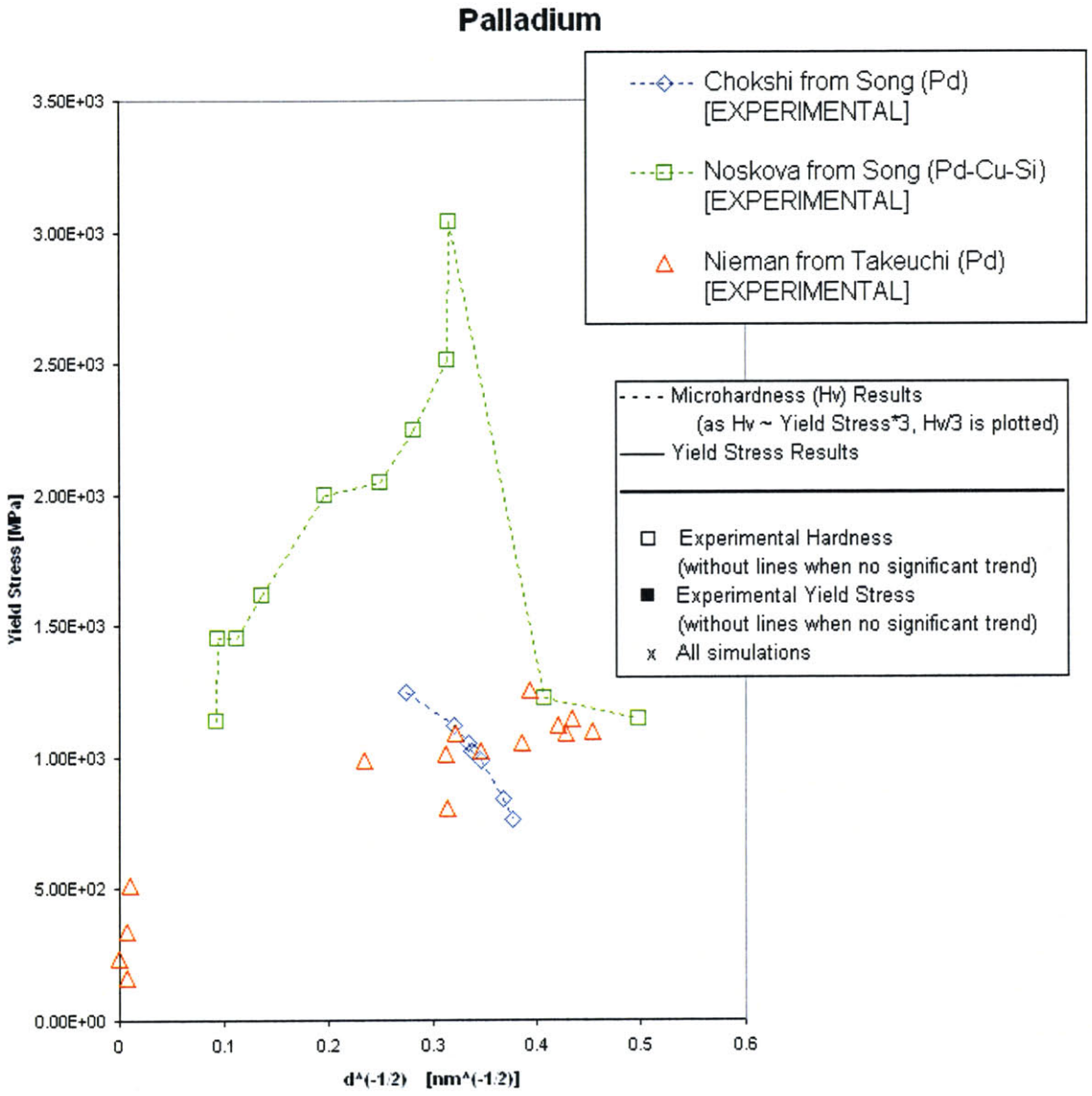

Figure A-2: Published results for the HP effects for palladium

will find examples in the PhD thesis of Jain [17] for steel (Figure A-3), in Sanders *et al.*'s publications [20, 21, 2] for copper (Figure A-1) and palladium (Figure A-2), in Furukawa *et al.*'s publications [32] for alloys of aluminum (Figure A-4), and in Hahn's publication [33] for alloys of titanium and aluminum (Figure A-5 and A-4). For transitions (clear or chaotic ones) and reverse HP effect, a summary of other authors' results can be found in Song's publications [10] for copper (Figure A-1), palladium (Figure A-2), and alloys of nickel-phosphorus (Figure A-6), iron-molybdenum-silicon-boron (Figure A-7) and palladium-copper-silicon (Figure A-2) or in Takeuchi's publication [34] for copper (Figure A-1) and palladium (Figure A-2). More recently, Haque's publication [18] presented results for aluminum noting that room temperature creep in his experiment was most probably negligible (Figure A-4). In 2003, Kumar, Van Swygenhoven and Suresh [1] published a very complete article on the attractive properties of nanocrystals concerning their strength, ductility and other properties, summing up the technological progress, related to experiments or molecular dynamics that are used to characterize their features. The same year, Kumar and Suresh *et al.* [35] were publishing another paper observing and identifying the deformation processes directly through state-of-the-art experiments, the same way, three years earlier, Agnew *et al.* [3] had presented their own observations. Finally, still in 2003, a promising paper on the influence of alloying on the strengthening (delaying the HP breakdown) was published by Schuh *et al.* [36] (Figure A-6).

It can be seen in the majority of these results that the general trend is a direct HP effect for the biggest size of grains, then some "flattening" with eventually a reverse HP effect. The discrepancies between all the curves for the same material can be explained by the fact that some nanocrystals may not have been (and were probably not) pure, under different temperature and pressure conditions. Consequently, depending of the porosity, the purity and the randomness of the orientation of the grains, results could vary significantly.

All experimental research is obviously not done on the reverse HP effect. Some is more oriented on optical or electrical properties of shape oriented nanocrystals [37] or on creep and temperature dependency phenomena [38, 39, 40].

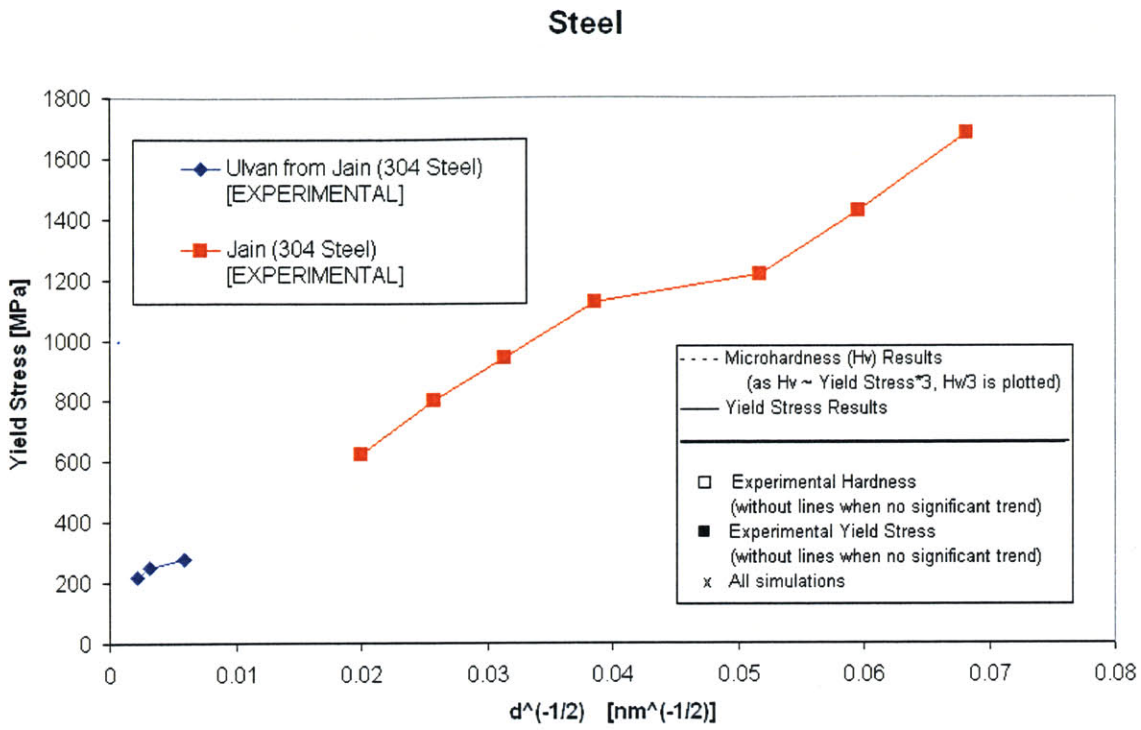

Figure A-3: Published results for the HP effects for steel

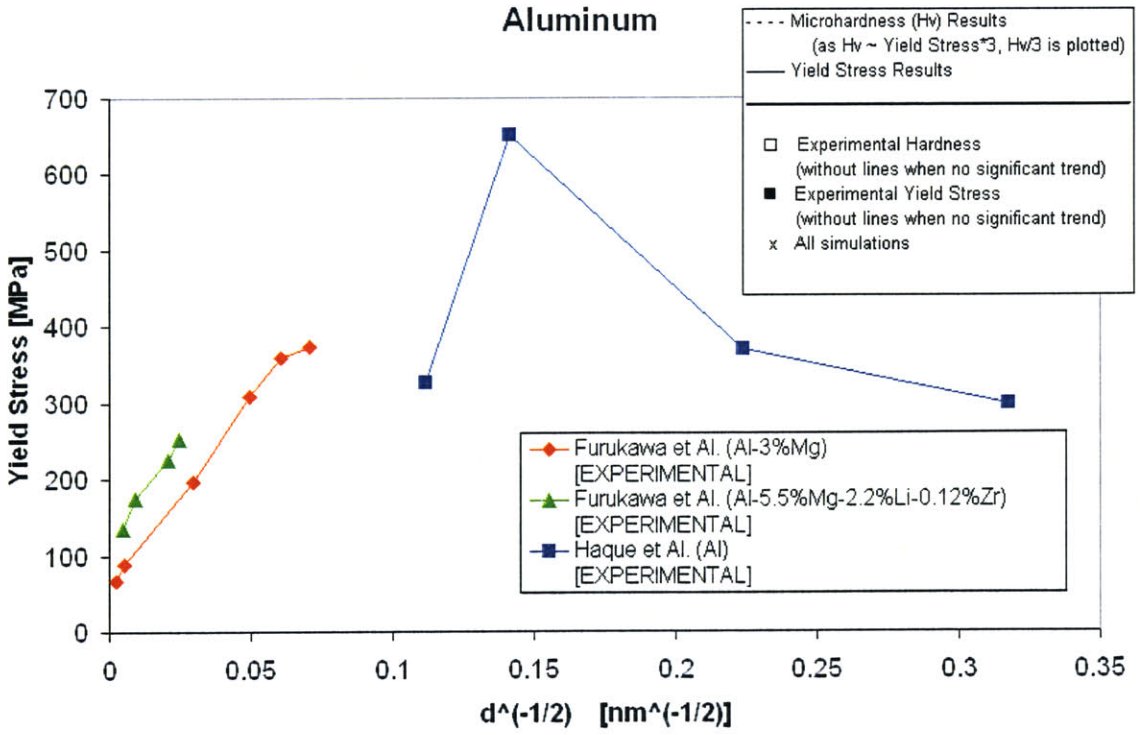

Figure A-4: Published results for the HP effects for aluminum

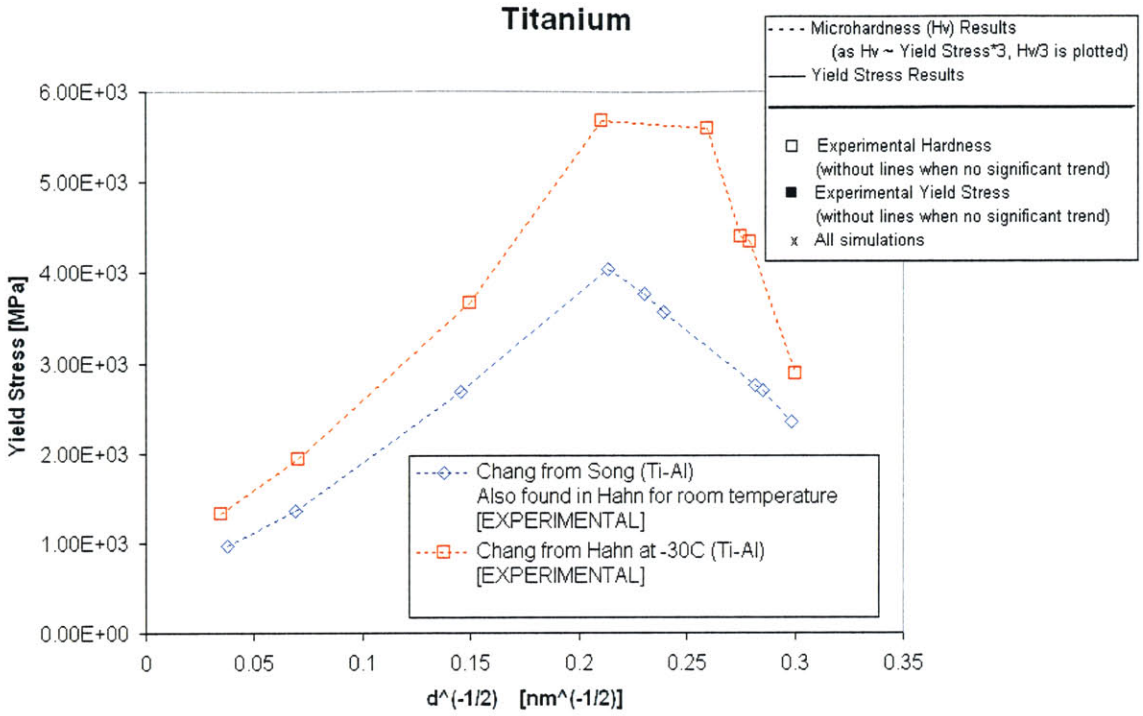

Figure A-5: Published results for the HP effects for titanium

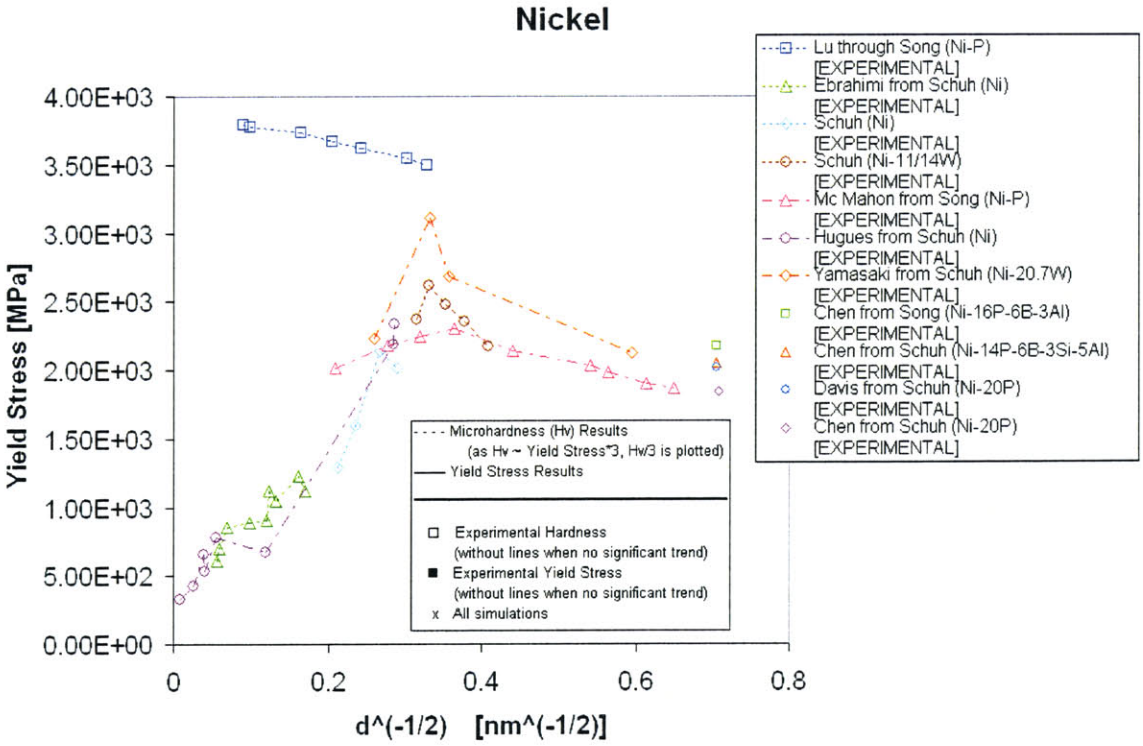

Figure A-6: Published results for the HP effects for nickel

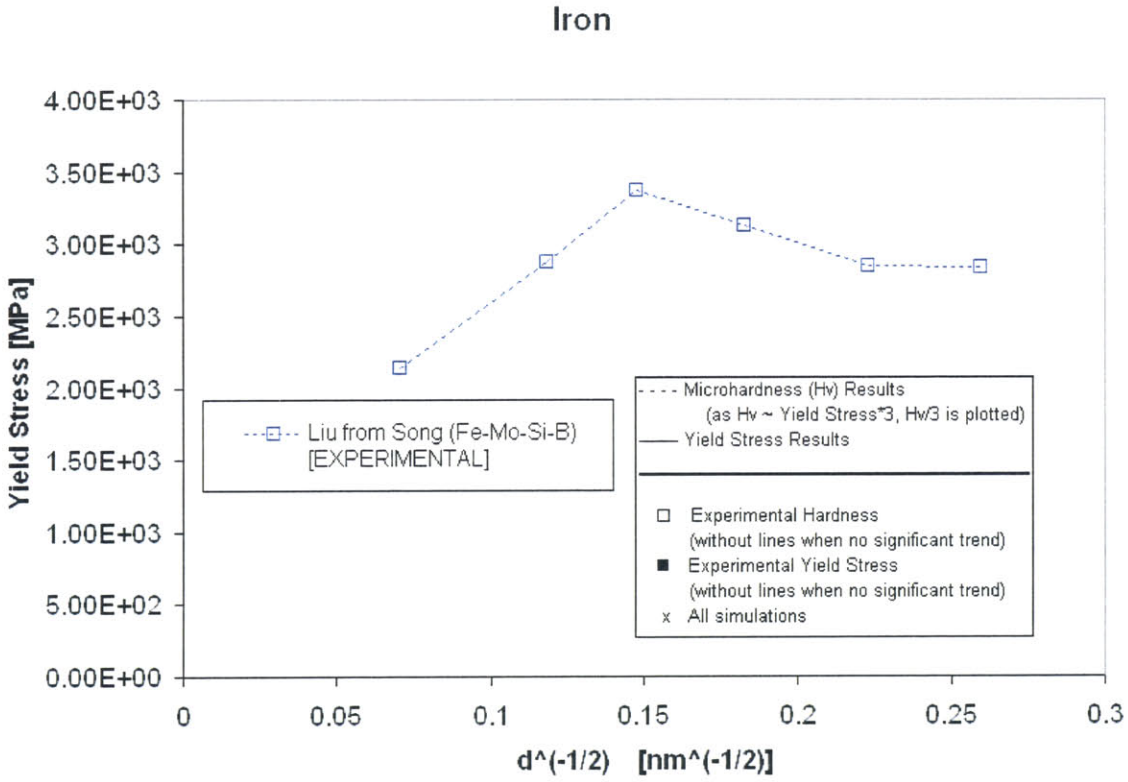

Figure A-7: Published results for the HP effects for iron

All these observations naturally incited people to find physical explanations and different theories. These theories influenced the following experiments, in a bilateral exchange.

A.2 Theories and hypotheses

The first theories on grain boundary sliding began to be published as early as the 1950s. In 1952, Rachinger [41] described the temperature dependency of the coupling between the non-directional growth of the grains, the tensile strain of each grain and the relative translatory movements (accounting for the difference between the individual strain of each grain and the global strain of the specimen). One of his conclusions was that slow-rate high-temperature deformation is mainly due to translatory movements. In 1963, Coble [42] published his famous paper describing the mechanism of grain boundary diffusion. The same year, Lifshitz gave his theory on the necessity of coupling between intragrain diffusion (the so called Nabarro-Herring diffusion) and grain boundary sliding. Eight years later, Stevens [23] continued this study by calculating the proportion of diffusion and sliding in a deformation for different shapes of grains. Looking at the problem the other way around, Raj and Ashby [43] studied how diffusion could be used to accommodate grain boundary sliding, using the work done by their predecessors. The next year Cannon [44] published a very interesting paper differentiating the grain boundary sliding whose purpose is to accommodate the strain (he called this "Rachinger grain boundary sliding") and the grain boundary sliding whose purpose is to accommodate diffusion (he called this "Lifshitz grain boundary sliding") and the proportion in which each one acts. In 1973, Ashby and Verrall [45] derived equations taking into account Coble and Nabarro-Herring diffusions.

All these publications were aiming at defining the importance of the fact that grain boundary sliding cannot occur by itself. A few decades later, people began to look more closely at the behavior of such phenomena for nanocrystals, discovering, with the help of innovations in technology allowing such observations, that they were one of the very important features of deformation at the nanoscale and were characterized

mainly by the reverse HP effect. For example, in 1997, Hahn and Padmanabhan [33] derived equations describing this effect (consequently *at the nanoscale*) insisting on the idea that grain boundary sliding was likely to be the main phenomenon of deformation and fitted their curves to Chang's results (see Figure A-5, the decreasing part of the curve corresponding to the room temperature). In a short paper published in Nature in 1998, Yip [12] recalled that such features were completely understandable by pointing out that grain boundary induced deformation and intragrain deformation were strongly length scale dependent, each one being predominant over the other on each side of a transition period corresponding to the break between direct and reverse HP effect. This remark was confirmed again the following year by Islamgaliev and Valiev [46] by experimental observation of high non-equilibrium activity at the grain boundary for ultrafine grains. The same year, Song, Guo and Hu [10] were fitting their model on the reverse HP effect curves of many experimental results (Figure A-5, A-7, A-2, A-1 and A-6). Their equations implied a $-\frac{1}{3}$ power dependency between yield stress and grain size. One of the biggest papers of 1999 is certainly Kê and Mehl's publication [25]. This publication essentially reviews all the studies done since 1947 concerning grain boundary relaxation. Chattopadhyay *et al.* [47], studying the phenomenon from a more thermodynamic point of view, published in 2000 a theory demonstrating the reverse HP effect. Lastly, a paper by Takeuchi [34] in 2001 can also be noticed for its model of shear deformation, calibrated using Schiøtz' results [11].

This quick review of the literature related to the different theories and explanations of nanocrystalline deformation is clearly not complete. Nevertheless, it can be considered as a basis for the development of an important effort towards simulation and modeling of this phenomenon, either in molecular dynamics or in another way.

A.3 Modeling and simulations

A.3.1 Molecular dynamics

The molecular dynamics simulations of grain boundary induced deformation began as early as the 1980s. Of course, the computational limitations were still important but a lot of basic features such as grain boundary sliding and grain boundary migration could already be studied. This is the case in two papers published by Bishop *et al.* [48, 49] in 1982 in which they studied migration, sliding, and annihilation of a bicrystal (the two crystals rotate in such a way that they finally switch into one unique crystal). This was also the case almost ten years later, with a study by Rickman *et al.* [50] on migration of a twist grain boundary. For both papers, sliding is considered as some accommodation process for migration. Both sets of simulations are not concerned with "pure" sliding of one crystal with respect to the other one but instead consider it as an accommodation process for migration. Sørensen *et al.* [51], in 1996, studied more specifically some simulations on sliding of one piece of crystal on another one, studying especially grain boundary energy and shear stress as a function of different intrinsic parameters. The same kind of study was also published by Molteni *et al.* the same year [52, 53]. In 1998, Schiøtz *et al.* [11] published results that would have quite a big impact in the field. By stretching a nanocrystal cube of 100,000 copper atoms, a clear reverse HP effect had been observed using grain size going from 6.56nm to 3.28nm. Furthermore, according to Schiøtz, diffusion did not play any important role during the deformation process. The following year, Van Swygenhoven *et al.* [54] were also observing by molecular dynamics the predominance, for nanocrystalline deformation, of grain boundary induced deformation (namely, sliding) over intragrain plasticity. This kind of observation directly at the grain boundary pushed researchers to try to understand the exact atomistic process that was occurring at the grain boundary, either by "traditional" molecular dynamics simulations on the role of defects at the grain boundary during sliding, as done by Kurtz *et al.* [55, 56], or with a different approach, such as Alexandrov's [57] where computer simulation of X-ray diffraction patterns have been used to investigate extrinsic grain boundary dislocation assemblies.

The year 1999 also saw the publication of another paper on Schiøtz *et al.*'s simulations [14] where temperature effects and defects features had been added to the publication of 1998 [11]. The same year, Van Swygenhoven *et al.* [13] also emphasized the switch between grain driven deformation and grain boundary driven deformation when reaching the nanoscale. In 2001, another similar set of simulations was done by Heino and Ristolainen [31], capturing in the same way the reverse HP effect. Still, the interest in the specific phenomena occurring at the grain boundary during migration and/or sliding did not decrease, as can be seen in the publications of Ballo *et al.* [58, 59, 60] or Van Swygenhoven and Derlet [61]. Other noteworthy publications from 2002 include work on grain boundary structure and resistance of Hoagland and Kurtz [62], some further studies on the influence of doping on sliding in aluminum bicrystal by Namilae *et al.* [63], a more creep/diffusion oriented publication and another on twinning in the deformation process by Yamakov *et al.* [64, 15], and finally three short publications by Schiøtz and Jacobsen [5, 16] on one hand, and Van Swygenhoven [6], on the other, with a much more philosophical approach of the problem, listing the limitations, advantages and future perspectives of MD and capturing, in Schiøtz' 2003 paper, the crossover between direct and reverse HP effect.

Not all simulations have been done using molecular dynamics. Different approaches have also been used in order to try to avoid the two main problems associated with this technique: the length scale and the time scale.

A.3.2 Other types of simulations

The two aforementioned limitations imply generally to work with molecular dynamics at very high strain rates using small specimens. Currently, one billion atom simulations have been made possible but a new limitation has risen: the huge amount of output information cannot be treated yet in an efficient manner. A natural alternative to this severe limitation is to consider other kind of simulations, namely FEM, or other techniques.

In 1994, Zhang *et al.* [65] created an FEM code with plastic grains and a rather simplistic approach of a grain boundary opening considered as two springs (one tan-

gential and one normal to the grain boundary) at the interstice. The results showed an interesting reorganization of the orientation of the crystals but the simplicity of the model was clearly a limitation to the application of this model to nanocrystalline deformation. In 1996 and 1997, Zikry and Kao [66, 67] published their results on the failure mechanisms at grain boundaries, concluding, with the help of an FEM formulation, that dislocation pile-ups were a direct cause of those failures. The same year, following these conclusions, Draheim and Gottstein [68] described their model of grain boundary migration based on the difference of dislocation density between two grains. This model gave some good results by comparison with some experiments, but a lack of energetic consideration (as opposed to geometric consideration) made the model unrealistic. Two years later, Onck and Van Der Giessen [69] published another study on the dependency of creep crack growth on grain size using an FEM approach. They concluded that creep crack growth increased with grain size. In 1999, Tokuda and Hu [70] reviewed different kinds of FEM features for different models, comparing and commenting on each one. Two years later, Shet *et al.* [71] published a comparison between FEM and MD explaining the pros and cons of both methods. In 2000 and 2003, Ashmawi and Zikry [72, 73] studied, using an FEM approach, more specific features such as mobile dislocations, immobile dislocations, or void porosity, and their influences on dislocation pile-ups at the grain boundary. Finally, Jiang and Weng [22] published their results in 2003 (see Figure A-1). Their specificities are due to the fact that a "composite model" (an approach considering the grain, the grain boundary around it, and the entire unit in a composite material representing the neighboring grains and their grain boundaries) has been used and fitted on experimental data (Sander's [20, 21]). Both direct and reverse HP effects have been captured and the observation that elasticity is the main intragrain deformation process for nanocrystals is given.

All these publications can now be considered as a good basis for a complete understanding of the features of deformation of nanocrystals. By coupling experimental knowledge, MD observations and FEM formulation, it is believed that a good and accurate approach of the nanocrystalline deformation can be mimicked. The clear

advantages of such an approach rely on the absence of severe limitations on strain rate and size (as for MD), nevertheless limited by the purely phenomenological descriptions of grain boundary deformation.

Bibliography

[1] K.S. Kumar, H. Van Swygenhoven and S. Suresh. Mechanical behavior of nanocrystalline metals and alloys. *Acta Materialia*, 51:5743–5774, 2003.

[2] C.J. Youngdahl, P.G. Sanders, J.A. Eastman and J.R. Weertman. Compressive yield strengths of nanocrystalline Cu and Pd. *Scripta Materialia*, 37:809–813, 1997.

[3] S.R. Agnew, B.R. Elliott, C.J. Youngdahl, K.J. Hemker and J.R. Weertman. Microstructure and mechanical behavior of nanocrystalline metals. *Materials Science and Engineering*, A285:391–396, 2000.

[4] H.V. Swygenhoven and J.R. Weertman. Preface to the viewpoint set on: mechanical properties of fully dense nanocrystalline metals. *Scripta Materialia*, 49:625–627, 2003.

[5] K.W. Jacobsen and J. Schiøtz. Nanoscale plasticity. *Nature Materials*, 1:15–16, 2002.

[6] H.V. Swygenhoven. Grain Boundaries and Dislocations. *Science*, 296(5565):66–67, 2002.

[7] E.O. Hall. The deformation and ageing of mild steel: III discussion of results. *Proceedings of the Physical Society of London*, B64:747–753, 1951.

[8] N.J. Petch. The cleavage strength of polycrystals. *Journal of the Iron and Steel Institute*, 174:25–28, 1953.

[9] A.H. Chokshi, A. Rosen, J. Karch and H. Gleiter. On the validity of the hall-petch relationship in nanocrystalline materials. *Scripta Mettalurgica*, 23:1679–1684, 1989.

[10] H.W. Song, S.R. Guo and Z.Q. Hu. A coherent polycrystal model for the inverse hall-petch relation in nanocrystalline materials. *NanoStructured Materials*, 11(2):203–210, 1999.

[11] J. Schiøtz, F.D. Di Tolla and K.W. Jacobsen. Softening of nanocrystalline metals at very small grain sizes. *Nature*, 391:561–563, 1998.

[12] S. Yip. The strongest size. *Nature*, 391:532–533, 1998.

[13] H. Van Swygenhoven, M. Spaczer, A. Caro, and D. Farkas. Competing plastic deformation mechanisms in nanophase metals. *Physical Review B-Condensed Matter*, 60(1):22–25, 1999.

[14] J. Schiøtz, T. Vegge, F.D. Di Tolla and K.W. Jacobsen. Atomic-scale simulations of the mechanical deformation of nanocrystalline metals. *Physical Review B*, 60(17):11971–11983, 1999.

[15] V. Yamakov, D. Wolf and S.R. Phillpot. Dislocation processes in the deformation of nanocrystalline aluminium by molecular-dynamics simulation. *Nature materials*, 1:1–4, 2002.

[16] J. Schiøtz and K.W. Jacobsen. A maximum in the strength of nanocrystalline copper. *Science*, 301:1357–1359, 2003.

[17] M.K. Jain. *Processing and Mechanical Behavior of Ultrafine Grain Materials.* PhD thesis, California Institute of Technology, 1995.

[18] M.A. Haque and M.T. A Saif. Mechanical behavior of 30-50 nm thick aluminum films under uniaxial tension. *Scripta Materiala*, 47:863–867, 2002.

[19] M. Ortiz and A. Pandolfi. Finite-deformation irreversible cohesive elements for three-dimensional crack-propagation analysis. *International Journal for Numerical Methods in Engineering*, 44:1267–1282, 1999.

[20] P.G. Sanders, J.A. Eastman and J.R. Weertman. Elastic and tensile behavior of nanocrystalline copper and palladium. *Acta Metallurgica*, 45:4019–4025, 1997.

[21] P.G. Sanders, C.J. Youngdhal and J.R. Weertman. The strength of nanocrystalline metals with and without flaws. *Materials Science and Engineering A*, 234-236:77–82, 1997.

[22] B. Jiang and G.J. Weng. A composite model for the grain-size dependence of yield stress of nanograins materials. *Metallurgical and Materials Transactions A*, 34A:765–772, 2003.

[23] R.N. Stevens. Grain-boundary sliding and diffusion creep in polycrystalline solids. *Philosophical Magazine*, 23:265–283, 1971.

[24] V. Yamakov, D. Wolf, S.R. Phillpot and H. Gleiter. Grain-boundary diffusion creep in nanocrystalline palladium by molecular-dynamics simulation. *Acta Materialia*, 50:61–73, 2002.

[25] T.S. Kê and R.F. Mehl. Fifty-year study of grain-boundary relaxation. *Metallurgical and Materials Transactions A*, 30A:2267–2295, 1999.

[26] R. Radovitzky and A. Cuitiño. Direct numerical simulation of polycrystals. In *44th AIAA/ASCE/ASME/AHS Structures, Structural Dynamics, and Materials Conference*, volume 1615. American Institute of Aeronautics and Astronautics, 2003.

[27] C. Teodosiu. *Elastic Models of Crystal Defects.* Springer-Verlag, New York, 1982.

[28] R. Radovitzky and M. Ortiz. Error estimation and adaptive meshing in strongly nonlinear dynamic problems. *Computer Methods In Applied Mechanics And Engineering*, 172(1-4):203–240, 1999.

[29] L. Stainier, A.M. Cuitino, and M. Ortiz. A micromechanical model of hardening, rate sensitivity and thermal softening in bcc single crystals. *Journal of the Mechanics and Physics of Solids*, 50(7):1511–1545, 2002.

[30] P. G. Ciarlet. *Numerical analysis of the finite element method.* Les Presses de L'Universite de Montreal, Quebec, Canada, 1976.

[31] P. Heino and E. Ristolainen. Strength of nanoscale polycristalline copper under shear. *Philosophical Magazine A*, 81(4):957–970, 2001.

[32] M. Furukawa, Z. Horita, M. Nemoto, R.Z. Valiev and T.G. Langdon. Factors influencing the flow and hardness of materials with ultrafine grain sizes. *Philosophical Magazine A*, 78(1):203–215, 1998.

[33] H. Hahn and K.A. Padmanabhan. A model for the deformation of nanocrystalline materials. *Philosophical Magazine B*, 76(4):559–571, 1997.

[34] S. Takeuchi. The mechanism of the inverse hall-petch relation of nanocrystals. *Scripta Materialia*, 44:1483–1487, 2001.

[35] K.S. Kumar, S. Suresh and M.F. Chisholm. Deformation of electrodeposited nanocrystalline nickel. *Acta Materialia*, 51:387–405, 2003.

[36] C.A. Schuh, T.G. Nieh and H. Iwasaki. The effect of solid solution W additions on the mechanical properties of nanocrystalline Ni. *Acta Materialia*, 51:431–443, 2003.

[37] X. Peng, L. Manna, W. Yang, J. Wickham, E. Scher, A. Kadavanich and A.P. Alivisatos. Shape control of CdSe nanocrystals. *Nature*, 404:59–61, 2000.

[38] N. Wang, Z. Wang, K.T. Aust and U. Erb. Room temperature creep behavior of nanocrystalline nickel produced by an electrodeposition technique. *Materials Sience and Engineering A*, 237:150–158, 1997.

[39] S.X. McFadden, R.S. Mishra, R.Z. Valiev, A.P. Zhilyaev and A.K. Mukherjee. Low-temperature superplasticity in nanostructured nickel and metal alloys. *Nature*, 398:684–686, 1999.

[40] W.M. Yin and S.H. Whang. Creep in boron-doped nanocrystalline nickel. *Scripta Materialia*, 44:569–574, 2001.

[41] W.A. Rachinger. Relative grain translations in the plastic flow of aluminium. *Journal of the Institute of Metals*, 81:33–41, 1952-53.

[42] R.L. Coble. A model for boundary diffusion controlled creep in polycrystalline materials. *Journal of Applied Physics*, 34(6):1679–1682, 1963.

[43] R. Raj and M.F. Ashby. On grain boundary sliding and diffusional creep. *Metallurgical Transactions*, 2:113–1127, 1971.

[44] W.R. Cannon. The contribution of grain boundary sliding to axial strain during diffusion creep. *Philosophical Magazine*, 25:1489, 1972.

[45] M.F. Ashby and R.A. Verrall. Diffusion-accommodated flow and superplasticity. *Acta Metallurgica*, 21:149–163, 1973.

[46] R.K. Islamgaliev and R.Z. Valiev. Non-equilibrium grain boundaries in ultrafine-grained materials processed by severe plastic deformation. *Materials Science Forum*, 294-296:361–364, 1999.

[47] P.P. Chattopadhyay, S.K. Pabi and I. Manna. On the inverse hall-petch relationship in nanocrystalline materials. *Zeitschrift für Metallkunde*, 91(12):1049–1051, 2000.

[48] G.H. Bishop Jr., R.J. Harrison, T. Kwok and S. Yip. Computer molecular-dynamics studies of grain-boundary structures. I. observations of coupled sliding and migration in a three-dimensional simulation. *Journal of Applied Physics*, 53(8):5596–5608, 1982.

[49] G.H. Bishop Jr., R.J. Harrison, T. Kwok and S. Yip. Computer molecular-dynamics studies of grain-boundary structures. II. migration, sliding, and annihilation in a two-dimensional solid. *Journal of Applied Physics*, 53(8):5609–5616, 1982.

[50] J.M. Rickman, S.R. Phillpot, D. Wolf, D.L. Woodraska and S. Yip. On the mechanism of grain-boundary migration in metals: A molecular dynamics study. *Journal of Materials Research*, 6(11):2291–2304, 1991.

[51] M.R. Sørensen, K.W. Jacobsen and P. Stoltze. Simulations of atomic-scale sliding friction. *Physical Review B*, 53(4):2101–2113, 1996.

[52] C. Molteni, G.P. Francis, M.C. Payne and V. Heine. First principles simulation of grain boundary sliding. *Physical Review Letters*, 76(8):1284–1297, 1996.

[53] C. Molteni, G.P. Francis, M.C. Payne and V. Heine. Grain boundary sliding: an ab initio simulation. *Materials Science and Engineering B*, 37:121–126, 1996.

[54] H. Van Swygenhoven, M. Spaczer and A. Caro. Microscopic description of plasticity in computer generated metallic nanophase samples: a comparison between Cu and Ni. *Acta Materialia*, 47(10):3117–3126, 1999.

[55] R.J. Kurtz, R.G. Hoagland and J.P. Hirth. Effect of extrinsic grain-boundary defects on grain-boundary sliding resistance. *Philosphical Magazine A*, 79(3):665–681, 1999.

[56] R.J. Kurtz, R.G. Hoagland and J.P. Hirth. Computer simulation of extrinsic grain-boundary defects in the $\Sigma 11, < 101 > \{131\}$ symmetric tilt boundary. *Philosophical Magazine A*, 79(3):683–703, 1999.

[57] I.V. Alexandrov, N.A. Enikeev and R.Z. Valiev. Investigation of assemblies of grain boundary dislocations in nanostructured copper by computer simulation. *Materials Science Forum*, 294-296:207–210, 1999.

[58] G. Lu and N. Kioussis. Interaction of vacancies with a grain boundary in aluminum: a first-principles study. *Physical Review B*, 64(024101):1–7, 2001.

[59] P. Ballo, N. Kioussis and G. Lu. Grain boundary sliding and migration: Effect of temperature and vacancies. *Physical Review B*, 64(024104):1–7, 2001.

[60] P. Ballo and V. Sluger̆. Atomic simulation of grain-boundary sliding and migration in copper. *Physical Review B*, 64(012107):1–3, 2001.

[61] H. Van Swygenhoven and P.M. Derlet. Grain-boundary sliding in nanocrystalline fcc metals. *Physical Review B*, 64(224105):1–9, 2001.

[62] R.G. Hoagland and R.J. Kurtz. The relation between grain-boundary structure and sliding resistance. *Philosophical Magazine A*, 82(6):1073–1092, 2002.

[63] S. Namilae, N. Chandra and T.G. Nieh. Atomistic simulation of grain boundary sliding in pure and magnesium doped aluminum bicrystals. *Scripta Materialia*, 46:49–54, 2002.

[64] V. Yamakov, D. Wolf, S.R. Phillpot and H. Gleiter. Grain-boundary diffusion creep in nanocrystalline palladium by molecular-dynamics simulation. *Acta Materialia*, 50:61–73, 2002.

[65] Y. Zhang, B.E. Hobbs and M.W. Jessell. The effect of grain-boundary sliding on fabric development in polycrystalline aggregates. *Journal of Structural Geology*, 16(9):1315–1325, 1994.

[66] M.A. Zikry and M. Kao. Inelastic microstructural failure mechanisms in crystalline materials with high angle grain boundaries. *Journal of the Mechanics and Physics of Solids*, 44(11):1765–1798, 1996.

[67] M.A. Zikry and M. Kao. Inelastic microstructural failure modes in crystalline materials: The $\Sigma 22A$ and $\Sigma 11$ high angle grain boundaries. *International Journal of Plasticity*, 13(4):403–434, 1997.

[68] K.J. Draheim and G. Gottstein. Simulation of grain boundary motion during high temperature cyclic deformation. *Computational Materials Science*, 7:208–212, 1996.

[69] P.R. Onck and E. van der Giessen. Numerical simulation of grain-size effects on creep crack growth by means of grain elements. *Journal de Physique IV*, 8:285–292, 1998.

[70] M. Tokuda and R. Hu. Finite element method simulation of grain boundary sliding: Its purposes, models and applications in fine-grain superplasticity. *Materials Science Forum*, 304-306:657–662, 1999.

[71] C. Shet, H. Li and N. Chandra. Interface models for gb sliding and migration. *Materials Science Forum*, 357-359:577–586, 2001.

[72] W.M. Ashmawi and M.A. Zikry. Effects of grain boundaries and dislocation density evolution on large strain deformation modes in fcc crystalline materials. *Journal of Computer-Aided Materials Design*, 7:55–62, 2000.

[73] W.M. Ashmawi and M.A. Zikry. Grain boundary effects and void porosity evolution. *Mechanics of Materials*, 35:537–552, 2003.